

Mechanistic Analysis of Double Hydrogen Dyotropy in *syn*-Sesquinorbornene Disulfones. A Combined Kinetic and Theoretical Evaluation of Primary Deuterium Isotope Effects

K. N. Houk,^{*1a} Yi Li,^{1a} Michael A. McAllister,^{1a} George O'Doherty,^{1b,2}
Leo A. Paquette,^{*1b} Willem Siebrand,^{*1c} and Zorka K. Smedarchina^{1c,3}

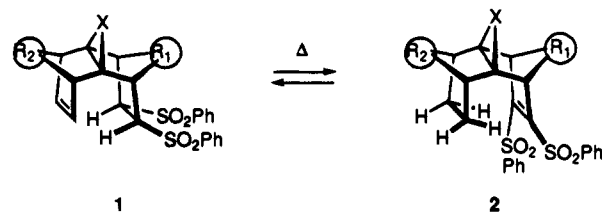
Contribution from the Departments of Chemistry, The University of California, Los Angeles, California 90024, and The Ohio State University, Columbus, Ohio 43210, and the Steacie Institute for Molecular Sciences, National Research Council of Canada, Ottawa, Ontario, Canada K1A 0R6

Received July 26, 1993[⊗]

Abstract: Two sets of *syn*-sesquinorbornene disulfones have been prepared that carry either one or two deuterium atoms α to the sulfonyl substituents. The rates of dyotropic rearrangement were measured in these systems in order to assess the deuterium isotope effects associated with single and double H/D transfer. The temperature dependence of the deuterium isotope effects in the bicyclopropane series **3b–5b** [$k_{HH}/k_{HD} = 5.4$ (0 °C) and 2.9 (100 °C); $k_{HH}/k_{DD} = 33$ (0 °C) and 8.5 (100 °C)] is not as steep as that when only one cyclopropane ring is present as in **3a–5a** [$k_{HH}/k_{HD} = 3.8$ (0 °C) and 2.1 (100 °C); $k_{HH}/k_{DD} = 200$ (0 °C) and 11.2 (100 °C)]. Only in the **b** series is the Rule of Geometric Mean obeyed. In an effort to gain detailed insight into the relationship between strain energy changes and rates of these reactions, the isomerization rates for a significant number of *syn*-sesquinorbornene disulfones were first modeled by means of the empirical MM3 force field. Good agreement was found based upon a concerted model. Transition structures for seven concerted dyotropic hydrogen transfers of *syn*-sesquinorbornene analogs were located with *ab initio* 3-21G calculations. The potential energy paths for concerted and stepwise hydrogen transfer were also evaluated at the CASSCF level of theory using minimum STO-3G and 3-21G basis sets. The concerted path is predicted to be favored in the absence of tunneling as in the **b** series. To take the tunneling effect into consideration, a more detailed dynamic treatment of the one- or two-dimensional barrier issue was next implemented. This model supports tunneling by a stepwise mechanism for both **3a–5a** and **3b–5b**, but the empirical energy parameters do not agree well with the best CASSCF calculations. Elaborate direct dynamics calculations on model compounds identical with **3a–5a** except for the phenylsulfonyl groups were carried out. Although they yielded results consistent with the two-oscillator calculations, the resulting activation energies are too low and leave room for some uncertainty about the mechanism, especially for compounds **3b–5b**.

Detailed understanding of the pathways adopted by intramolecular atom transfer reactions has commanded considerable recent attention because of possible existing relationships to the mechanism of enzyme action.⁴ In an effort to obtain quantitative data on the extent to which geometric disposition impacts on chemical reactivity, Mackenzie⁵ and Paquette⁶ have undertaken experiments in which rates of double hydrogen dyotropic

migration have been correlated directly to the distance separating the reaction centers. The Ohio State group prepared a series of *syn*-sesquinorbornene disulfones **1** in which the intracavity gap was appreciably varied by suitable modification of the regions defined as R₁ and R₂, as well as the group X in the central core. Significantly, the distances separating the α -sul-



fonyl hydrogens and the nearby olefinic carbons were found not to correlate well with the isomerization rate constants. Instead, the observed reactivity pattern conformed much better to the variations in strain between ground and transition states.⁶

A still more fundamental issue is the concerted or stepwise nature of such double hydrogen transfers. Although the potential concertedness of $\sigma_{2s} + \sigma_{2s} + \pi_{2s}$ processes has been recognized for some time,⁷ early theoretical studies predicted a barrier of 71 kcal/mol for the concerted exchange of hydrogen between

[⊗] Abstract published in *Advance ACS Abstracts*, November 1, 1994.

(1) (a) The University of California, Los Angeles. (b) The Ohio State University. (c) The National Research Council of Canada.

(2) BP America Fellow, 1991; National Needs Fellow, 1989–1990; University Fellow, 1988–1989.

(3) NRCC Visiting Scientist. Permanent address: Institute of Organic Chemistry, Bulgarian Academy of Sciences, 1113 Sofia, Bulgaria.

(4) (a) Page, M. I. In *Enzyme Mechanisms*; Page, M. I., Williams, A., Eds.; Royal Society of Chemistry: London, 1987. (b) Czamik, A. W. In *Mechanistic Principles of Enzyme Activity*; Liebman, J. F., Greenberg, A., Eds.; VCH Publishers, Inc.: New York, 1986. (c) Fersht, A. P. *Enzyme Structure and Mechanism*, 2nd ed.; Freeman: San Francisco, 1984.

(5) (a) Mackenzie, K.; Howard, J. A. K.; Mason, S.; Gravett, E. C.; Astin, K. B.; Liu, S.-X.; Batsanov, A. S.; Vlaovic, D.; Maher, J. P.; Murray, M.; Kendrew, D.; Wilson, D.; Johnson, R. E.; Preiss, T.; Gregory, R. J. *J. Chem. Soc., Perkin Trans. 2* **1993**, 1211. (b) Mackenzie, K.; Gravett, E. C.; Gregory, R. J.; Howard, J. A. K.; Maher, J. P. *Tetrahedron Lett.* **1992**, 33, 5629. (c) Howard, J. A. K.; Mackenzie, K.; Johnson, R. E.; Astin, K. B. *Tetrahedron Lett.* **1989**, 30, 5005. (d) Geich, H.; Grimme, W.; Proske, K. *J. Am. Chem. Soc.* **1992**, 114, 1492.

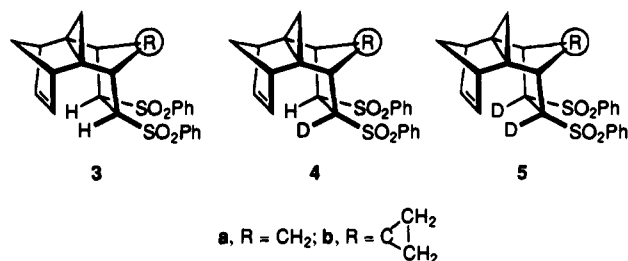
(6) (a) Paquette, L. A.; Kesselmayr, M. A.; Rogers, R. D. *J. Am. Chem. Soc.* **1990**, 112, 284. (b) Paquette, L. A.; O'Doherty, G. A.; Rogers, R. D. *J. Am. Chem. Soc.* **1991**, 113, 7761. (c) O'Doherty, G. A.; Rogers, R. D.; Paquette, L. A. *J. Am. Chem. Soc.*, preceding paper in this issue.

(7) (a) Reetz, M. T. *Angew. Chem., Int. Ed. Engl.* **1972**, 11, 129. (b) Reetz, M. T. *Tetrahedron* **1973**, 29, 2189.

ethane and ethylene.⁸ More recent computational work strongly suggests, however, that thermoneutral concerted hydrogen transfers should proceed with relatively low activation energies and therefore bypass stepwise alternatives.^{9,10} However, it has been recognized for some time that processes involving hydrogen transfer differ from most other chemical transformations in that they often behave nonclassically¹¹ via quantum-mechanical tunneling.^{12–15} A notable application of this model can be found in the asynchronous transfer of hydrogen within free-base porphyrins.¹⁶ In order to elucidate the mechanism of the 1 → 2 conversion, deuterium isotope effect studies have now been undertaken. MCSCF calculations have also been performed on dihydrogen transfers by concerted and stepwise mechanisms for the parent systems. RHF/3-21G calculations on various derivatives were also performed. Further, an MM3 force field has been elaborated for the transition structures of these dyotropic reactions based upon the geometries of *ab initio* 3-21G transition structures for the dyotropic hydrogen transfer reaction between ethane and ethylene. Finally, a quantitative analysis of the experimental kinetic isotope effects was performed with both model Golden Rule and direct dynamics calculations.

Results and Discussion

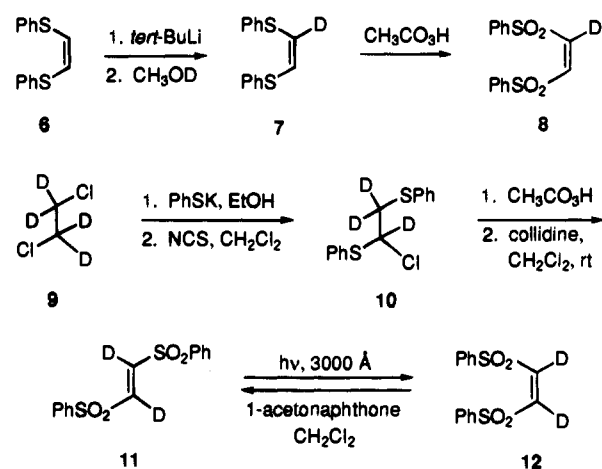
Synthetic Considerations. The six disulfones **3a**, **4a**, **5a** and **3b**, **4b**, **5b** were targeted for direct kinetic comparison. Acquisition of the *d*₁ substrates began by reaction of (*Z*)-1,2-bis(phenylthio)ethylene (**6**)¹⁷ with *tert*-butyllithium at 100 °C.¹⁸



Quenching of the monoanion so produced with CH₃OD at –78 °C afforded **7** (92% *d*₁ by ¹H NMR analysis), oxidation of which with peracetic acid produced **8** without loss of isotopic content.¹⁹ Diels–Alder addition of this dienophile to the proper tricyclo-[5.2.1.0^{2,6}]deca-2,5,8-triene and regiospecific cyclopropanation of the central double bond in the adducts as before⁶ produced **4a** and **4b**.

Successful arrival at dideuterated disulfone **12** proved to be far more problematical. Repeated deprotonation–deuteration of **7** in an effort to produce the *d*₂-sulfide was not practical because β-elimination to yield phenylthiopyne competed

effectively. Attempts to promote the Michael addition of PhSD to either (phenylthio)acetylene-*d*₁ or (phenylsulfonyl)acetylene-*d*₁ proved entirely unrewarding. An alternative retro-Diels–Alder route²⁰ was foiled because exposure of the anthracene–1,2-bis(phenylsulfonyl)acetylene adduct to D₂ in the presence of Pd/C resulted only in the saturation of one of the aromatic rings. When still other routes to **12** failed,²¹ attention was turned to producing preliminarily the dideuterated *E*-disulfone **11** from commercially available 1,2-dichloroethane-*d*₄ (**9**). Following 2-fold S_N2 displacement with potassium thiophenoxide, monochlorination was easily achieved with *N*-chlorosuccinimide²² to give **10**. Subsequent peracetic acid oxidation and dedeuteriochlorination with collidine²³ proceeded smoothly. Irradiation of CH₂Cl₂ solutions of **11** in the presence of 1-acetonaphthone as sensitizer²⁴ permitted the establishment of a photoequilibrium favoring **11** (3:1) after 2 days.²⁵ The geometric isomers were conveniently separated by MPLC on silica gel, thereby permitting the recycling of **11**. Disulfone **12** so obtained (>99% *d*₂



by ¹H NMR analysis) served as the precursor to **5a** and **5b**.

Kinetic Measurements. The selection of **3a** and **3b** and their deuterated analogs as suitable mechanistic probes was predicated on their differing intragap distance, the nonidentity of prevailing steric congestion in their α_a and α_b zones,^{6c} and the dissimilarity of their relative dyotropic rearrangement rates.^{6c} As a consequence, kinetic measurements across the **a** series were necessarily conducted over the 100–130 °C temperature range, while the rate studies involving the more reactive **b** series were undertaken at 50–100 °C. The relevant absolute rate data and activation parameters are summarized in Tables 1 and 2.

The experimentally derived *K*_{eq} for **4a** and **4b** with their respective dyotropomers were found to be identical within experimental error to those of **3a** and **3b**, respectively. Consequently, the mole fractions of the *d*₀ and *d*₁ species contribute directly to *k*_{obsd} as shown in eq 1. Simple subtraction of the

$$0.92k_{\text{HD}} + 0.08k_{\text{HH}} = k_{\text{obsd}} \quad (1)$$

appropriately factored rate constants for **3a** and **3b** from the

(20) Sweger, R. W.; Czamik, A. W. In *Comprehensive Organic Synthesis*, Trost, B. M., Fleming, I., Eds.; Pergamon Press: Oxford, 1991; Chapter 4.5.

(21) Relevant analogy may be found in the following reports: (a) Bjorlo, O.; Verkrujssse, H. D.; Brandsma, L. *Synth. Commun.* **1992**, *22*, 1563. (b) Sauer, J.; Wiest, H.; Mielert, A. *Chem. Ber.* **1964**, *97*, 3183.

(22) Paquette, L. A.; Klobucar, W. D.; Snow, R. S. *Synth. Commun.* **1976**, *6*, 575.

(23) DeLucchi, O.; Lucchini, V.; Pasquato, L.; Modena, G. *J. Org. Chem.* **1984**, *49*, 596.

(24) Other sensitizers were less effective. For precedent, see: Swenton, J. S.; Gates, B. D. *Tetrahedron Lett.* **1992**, *33*, 2127.

(25) The reaction mixture develops a brown color at this point rendering further irradiation unproductive. When **12** was irradiated under identical conditions, a 1:1 ratio of *E/Z* isomers resulted.

(8) Feller, D. F.; Schmidt, M. W.; Ruedenberg, K. *J. Am. Chem. Soc.* **1982**, *104*, 960.

(9) McKee, M. L.; Stanbury, D. M. *J. Am. Chem. Soc.* **1992**, *114*, 3214.

(10) Jensen, F. *J. Am. Chem. Soc.* **1992**, *114*, 1596.

(11) (a) Siebrand, W.; Wildman, T. A.; Zgierski, M. Z. *J. Am. Chem. Soc.* **1984**, *106*, 4083. (b) Siebrand, W.; Wildman, T. A.; Zgierski, M. Z. *J. Am. Chem. Soc.* **1984**, *106*, 4089.

(12) (a) Bell, R. P. *The Tunnel Effect in Chemistry*; Chapman and Hall: London, 1980. (b) Melander, L.; Saunders, W. H., Jr. *Reaction Rates of Isotopic Molecules*; Wiley: New York, 1980; p 209 ff and references cited therein.

(13) Johnston, H. S. *Adv. Chem. Phys.* **1960**, *3*, 131.

(14) Caldin, E. G. *Chem. Rev.* **1969**, *69*, 135.

(15) Harmony, M. D. *Chem. Soc. Rev.* **1972**, *1*, 211.

(16) Smedarchina, Z.; Siebrand, W.; Zerbetto, F. *Chem. Phys.* **1989**, *136*, 285.

(17) (a) Truce, W. E.; McManimie, R. J. *J. Am. Chem. Soc.* **1954**, *76*, 5745. (b) Parham, W. E.; Heberling, J. J. *J. Am. Chem. Soc.* **1955**, *77*, 1175.

(18) Schmidt, R. R.; Schmid, B. *Tetrahedron Lett.* **1977**, 3583.

(19) Paquette, L. A.; Künzer, H.; Kesselmayer, M. A. *J. Am. Chem. Soc.* **1988**, *110*, 6521.

Table 1. Absolute Rate Data, Activation Parameters, and Deuterium Isotope Effects for Double Hydrogen (Deuterium) Dyotropy in **3a**, **4a**, and **5a**

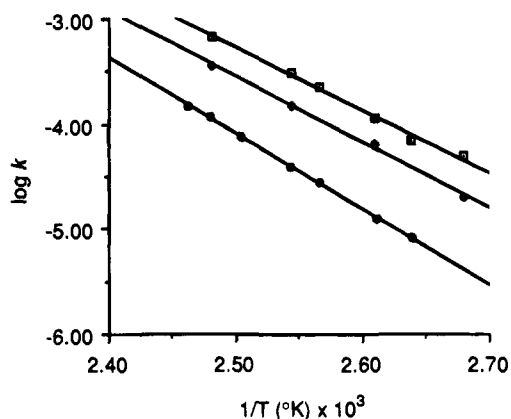
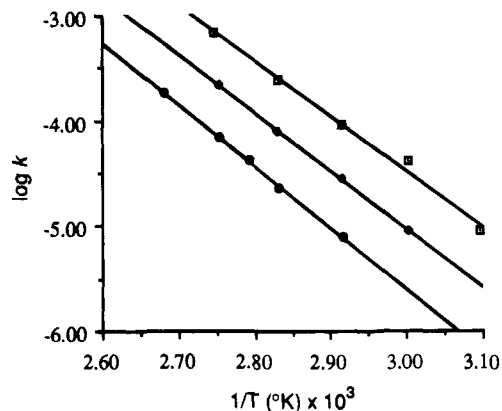
compd	T, °C	k, s ⁻¹	log k	k _H /k _D
3a	100.0 ± 0.5	(5.06 ± 0.25) × 10 ⁻⁵	-4.296	1.0
	106.5 ± 0.5	(7.11 ± 0.36) × 10 ⁻⁵	-4.148	
	110.0 ± 0.5	(1.15 ± 0.06) × 10 ⁻⁴	-3.939	
	116.5 ± 0.5	(2.24 ± 0.11) × 10 ⁻⁴	-3.650	
	120.0 ± 0.5	(3.07 ± 0.15) × 10 ⁻⁴	-3.513	
	130.0 ± 0.5	(6.93 ± 0.35) × 10 ⁻⁵	-3.159	
	100 ^a	4.58 × 10 ⁻⁵		
0 ^a	6.71 × 10 ⁻¹¹			
4a	100.0 ± 0.5	(2.04 ± 0.10) × 10 ⁻⁵	-4.690	2.1 (100 °C) 3.8 (0 °C)
	110.0 ± 0.5	(6.49 ± 0.32) × 10 ⁻⁵	-4.188	
	120.0 ± 0.5	(1.52 ± 0.08) × 10 ⁻⁵	-3.819	
	130.0 ± 0.5	(3.61 ± 0.18) × 10 ⁻⁴	-3.442	
	100 ^a	2.17 × 10 ⁻⁵		
	0 ^a	1.75 × 10 ⁻¹¹		
	5a	106.5 ± 0.5	(8.32 ± 0.42) × 10 ⁻⁶	
110.0 ± 0.5		(1.29 ± 0.06) × 10 ⁻⁵	-4.891	
116.5 ± 0.5		(2.80 ± 0.14) × 10 ⁻⁵	-4.553	
120.0 ± 0.5		(4.05 ± 0.20) × 10 ⁻⁵	-4.393	
126.0 ± 0.5		(7.74 ± 0.39) × 10 ⁻⁵	-4.111	
130.0 ± 0.5		(1.14 ± 0.06) × 10 ⁻⁴	-3.942	
133.0 ± 0.5		(1.51 ± 0.08) × 10 ⁻⁴	-3.821	
100 ^a		4.10 × 10 ⁻⁶		
0 ^a		3.35 × 10 ⁻¹³		

for **3a**: $\Delta H^\ddagger_{(25^\circ\text{C})} = 26.6 \pm 1.0$ kcal/mol
 $\Delta G^\ddagger_{(25^\circ\text{C})} = 28.8 \pm 2.0$ kcal/mol
 $\Delta S^\ddagger_{(25^\circ\text{C})} = -7.3 \pm 2.6$ eu
 $E_a = 27.2 \pm 2.0$ kcal/mol
 $\log A = 11.6 \pm 0.06$

for **4a**: $\Delta H^\ddagger_{(25^\circ\text{C})} = 27.8 \pm 1.0$ kcal/mol
 $\Delta G^\ddagger_{(25^\circ\text{C})} = 29.5 \pm 2.0$ kcal/mol
 $\Delta S^\ddagger_{(25^\circ\text{C})} = -5.6 \pm 2.6$ eu
 $E_a = 28.4 \pm 2.0$ kcal/mol
 $\log A = 12.0 \pm 0.6$

for **5a**: $\Delta H^\ddagger_{(25^\circ\text{C})} = 32.5 \pm 1.2$ kcal/mol
 $\Delta G^\ddagger_{(25^\circ\text{C})} = 31.5 \pm 2.0$ kcal/mol
 $\Delta S^\ddagger_{(25^\circ\text{C})} = 3.5 \pm 3.0$ eu
 $E_a = 33.1 \pm 2.2$ kcal/mol
 $\log A = 14.0 \pm 0.7$

^a Extrapolated rate constants.

**Figure 1.** Arrhenius plot for **3a** (□), **4a** (◆), and **5a** (○).**Figure 2.** Arrhenius plot for **3b** (□), **4b** (◆), and **5b** (○).

k_{obsd} values for **4a** and **4b**, respectively, gave rise to the data compiled in Tables 1 and 2. In all cases, excellent linearity was realized in the Arrhenius plots (Figures 1 and 2). As a consequence, the extrapolation of these data to 25 °C and 100 °C is considered to be very reliable. It is of course well-known that transfer rate constants involving tunneling give rise to curved Arrhenius plots; any leveling off would occur at higher temperatures for hydrogen than for deuterium, which would give rise to a further increase of the deuterium effect at lower temperatures.²⁶

For the monocyclopropane series, the $k_{\text{HH}}/k_{\text{HD}}$ ratios are calculated to be 3.8 (0 °C) and 2.1 (100 °C), while those for

$k_{\text{HH}}/k_{\text{DD}}$ are significantly larger at 200 (0 °C) and 11.2 (100 °C). The temperature dependence of the deuterium isotope effects in the bicyclopropane triad is not as steep, with $k_{\text{HH}}/k_{\text{HD}}$ being 5.4 (0 °C) and 2.9 (100 °C) and $k_{\text{HH}}/k_{\text{DD}}$ amounting to 33 (0 °C) and 8.5 (100 °C).

As concerns **3a–5a**, the magnitudes of $k_{\text{HH}}/k_{\text{DD}}$ greatly exceed those for $[k_{\text{HH}}/k_{\text{HD}}]^2$: 11.2 vs $[2.1]^2 = 4.4$ at 100 °C and 200 vs $[3.8]^2 = 14.4$ for data extrapolated to 0 °C. These findings are inconsistent with the Rule of Geometric Mean²⁷ and suggest that asymmetrical transition states are operative. Thus, we see that the isotope effect for the first D is 2.1 at 100 °C, while that for the second D (viz., $k_{\text{HD}}/k_{\text{DD}}$) is 5.3. The corresponding

(26) See ref 12. Thus the isotope effect of 200 may well be an underestimate.

(27) See ref 12b, p 209, and Bigeleisen, J. J. Chem. Phys. 1955, 23, 2264.

Table 2. Absolute Rate Data, Activation Parameters, and Deuterium Isotope Effects for Double Hydrogen (Deuterium) Dyotropy in **3b**, **4b**, and **5b**

compd	T, °C	k, s ⁻¹	log k	k _H /k _D
3b	50.0 ± 0.5	(9.02 ± 0.45) × 10 ⁻⁶	-5.045	1.0
	60.0 ± 0.5	(4.11 ± 0.21) × 10 ⁻⁵	-4.386	
	70.0 ± 0.5	(9.08 ± 0.45) × 10 ⁻⁵	-4.042	
	80.0 ± 0.5	(2.47 ± 0.12) × 10 ⁻⁴	-3.607	
	91.0 ± 0.5	(6.93 ± 0.35) × 10 ⁻⁴	-3.159	
	100 ^a	1.59 × 10 ⁻³		
	0 ^a	1.11 × 10 ⁻⁸		
4b	60.0 ± 0.5	(9.08 ± 0.45) × 10 ⁻⁶	-5.042	2.9 (100 °C) 5.4 (0 °C)
	70.0 ± 0.5	(2.85 ± 0.14) × 10 ⁻⁵	-4.545	
	80.0 ± 0.5	(7.83 ± 0.39) × 10 ⁻⁵	-4.106	
	90.0 ± 0.5	(2.16 ± 0.11) × 10 ⁻⁴	-3.665	
	100 ^a	5.51 × 10 ⁻⁴		
	0 ^a	2.07 × 10 ⁻⁹		
5b	70.0 ± 0.5	(7.96 ± 0.40) × 10 ⁻⁶	-5.099	8.5 (100 °C) 33 (0 °C)
	80.0 ± 0.5	(2.37 ± 0.12) × 10 ⁻⁵	-4.626	
	85.0 ± 0.5	(4.21 ± 0.21) × 10 ⁻⁵	-4.376	
	90.0 ± 0.5	(6.95 ± 0.35) × 10 ⁻⁴	-4.158	
	100.0 ± 0.5	(1.86 ± 0.09) × 10 ⁻⁴	-3.731	
	100 ^a	1.86 × 10 ⁻⁴		
	0 ^a	3.37 × 10 ⁻¹⁰		

for 3b : $\Delta H^\ddagger_{(25^\circ\text{C})} = 23.5 \pm 0.6$ kcal/mol	for 4b : $\Delta H^\ddagger_{(25^\circ\text{C})} = 24.7 \pm 0.8$ kcal/mol
$\Delta G^\ddagger_{(25^\circ\text{C})} = 26.1 \pm 1.2$ kcal/mol	$\Delta G^\ddagger_{(25^\circ\text{C})} = 26.9 \pm 1.6$ kcal/mol
$\Delta S^\ddagger_{(25^\circ\text{C})} = -8.7 \pm 1.7$ eu	$\Delta S^\ddagger_{(25^\circ\text{C})} = -7.5 \pm 2.3$ eu
$E_a = 24.1 \pm 1.1$ kcal/mol	$E_a = 25.3 \pm 1.8$ kcal/mol
$\log A = 11.3 \pm 0.4$	$\log A = 11.6 \pm 0.5$

for 5b : $\Delta H^\ddagger_{(25^\circ\text{C})} = 26.2 \pm 0.9$ kcal/mol
$\Delta G^\ddagger_{(25^\circ\text{C})} = 27.9 \pm 1.8$ kcal/mol
$\Delta S^\ddagger_{(25^\circ\text{C})} = -5.7 \pm 2.4$ eu
$E_a = 26.8 \pm 1.8$ kcal/mol
$\log A = 12.0 \pm 0.5$

^a Extrapolated rate constants.

values at 0 °C are 3.8 and 53. The Arrhenius plots for **3a** and **4a** give $A_{\text{HH}}/A_{\text{HD}} = 0.4$. The $A_{\text{HH}}/A_{\text{DD}}$ value for **3a/5a** is 0.004, suggesting that quantum mechanical tunneling is occurring. Of course, $A_{\text{HH}}/A_{\text{HD}}$ and $A_{\text{HH}}/A_{\text{DD}}$ values smaller than unity are a physical anomaly since the lighter particle should have the higher frequency factor. This anomaly arises in curved Arrhenius plots associated with tunneling since the temperature of maximum curvature is lower for heavier particles. It therefore provides additional evidence that tunneling takes place. For the bicycloprenes **4b** and **5b**, the rate is increased at 100 °C by a factor of 35. The A-factor ratios in these examples are much closer to unity (0.5, 0.2), despite the closer proximity of the α -sulfonyl protons to the olefinic carbons in **3b** (2.25 Å) relative to **3a** (2.32 Å).⁶ The most important factors, of course, are the respective barrier heights and, as we show, the lower the barrier height the less tunneling.^{28,29} Stated differently, when the activation energy required for distortion of the heavy atoms to bring the reacting hydrogen to a nontunneling distance is greater, there is more room for compensating tunneling.

Ab Initio Study of the Concerted Dihydrogen Transfer. Because of the size of the systems studied, we could neither perform the calculations on the real disubstituted systems nor do the calculations at the highest available level of theory. We performed the calculations at the RHF level on systems lacking the sulfone substituents, using the 3-21G basis set.³⁰ The basis

(28) (a) For a recent attempt to establish the concerted/nonconcerted mechanism of a dyotropic (6 + 4)-hydrogen migration, consult ref 5d. (b) Schowen, R. L. Private communication (Oct 10, 1992).

(29) A referee has raised concern over the fact that the reported k values might include the sum of the forward and reverse rate constants as $k = k_f + k_r = k_f(1 + K_{\text{eq}}^{-1})$. As indicated in the preceding paper, this is not the case. Furthermore, since equilibrium isotope effects near unity were found, there will be no influence of K_{eq} on the isotope effects. Neither is it a problem for the rate constants, since only k_f were determined and ultimately used in the comparisons with theory.

set is known to give reasonable hydrocarbon geometries, but RHF theory is biased toward a concerted mechanism. We overcame this bias by performing CASSCF calculations described later.

Figure 3 shows the optimized transition state geometries for the parent system and the analogs listed in Table 3. There is a remarkable resemblance between these which is displayed in the two structures in Figure 4. The structures are superpositions of the transition states for *syn*-sesquinorborene and analogs on the transition state for the ethane-ethylene reaction. Some C-H-C bending is necessitated by the skeleton, but otherwise there are very great similarities among the various transition states.

The reactant structures are shown in Figure 5. These are superimposed in Figure 6, which has the ethano bridges overlaid. The etheno bridges are quite displaced in space from each other. As shown in Table 3, the structures with the transferring C-H and the alkene furthest removed are predicted to have the highest activation energies. These require the most energy to distort to the transition state, or in the tunneling model described later, to the geometry required for tunneling. The predicted activation energies range from 30.9 to 47.9 kcal/mol, all somewhat smaller than the 50.8 kcal/mol calculated for the ethane-ethylene reaction.

Further evidence for the concerted path is provided from the good structure-reactivity correlation obtained on the basis of the concerted synchronous path (Table 3). For the concerted transition structures of pericyclic reactions, we have shown that calculations at the restricted HF (RHF) level of theory with the 3-21G basis set give geometries comparable to those calculated at higher levels.³¹ Here, we calculated reaction barriers for a

(30) Binkley, J. S.; Pople, J. A.; Hehre, W. J. *J. Am. Chem. Soc.* **1980**, *102*, 939.

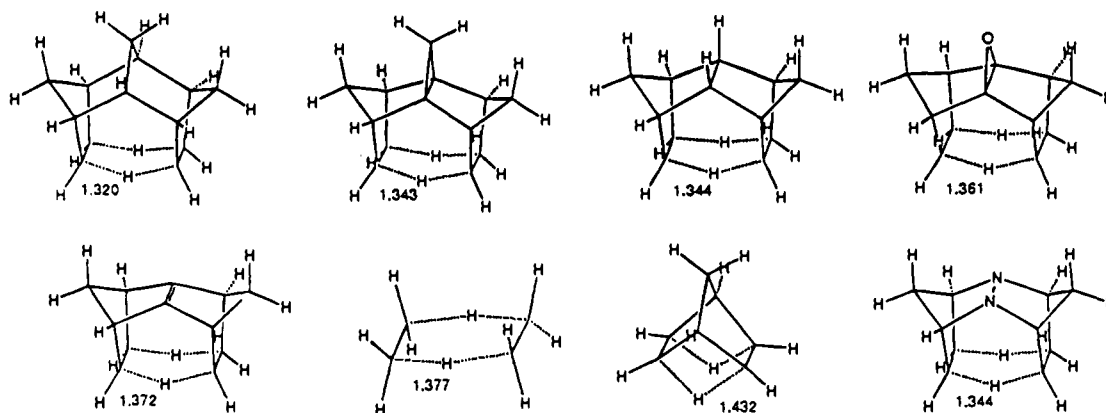


Figure 3. RHF/3-21G transition structures for the double hydrogen dyotropy reactions.

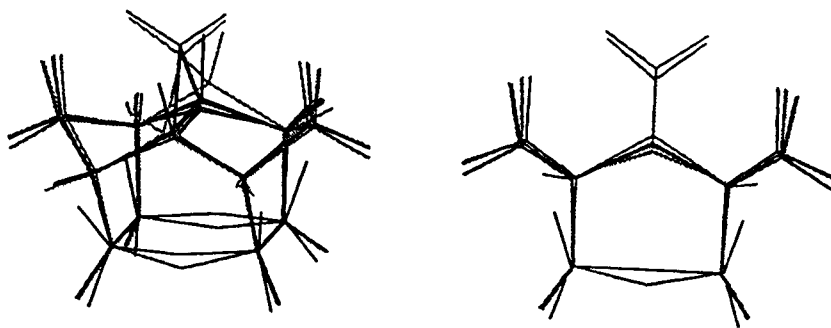


Figure 4. Superimposition of the RHF/3-21G transition structures.

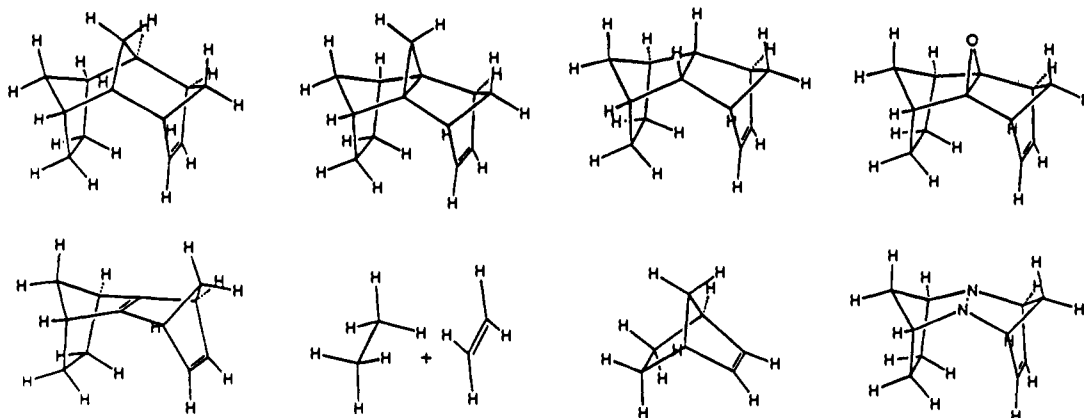


Figure 5. RHF/3-21G reactants of double hydrogen dyotropy reactions.

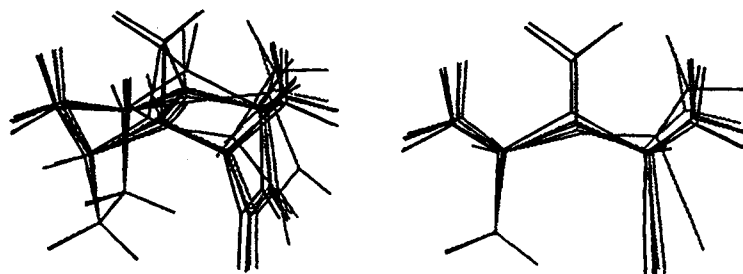
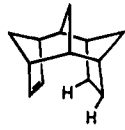


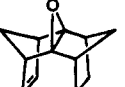

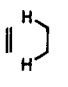
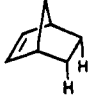



Figure 6. Superimposition of the RHF/3-21G reactants.

series of concerted intramolecular double hydrogen transfer reactions at the correlated MP2 level of theory using the RHF/3-21G geometries. The results are summarized in Table 3. For the thermal neutral reactions of sesquinorbornenes, the order of calculated intrinsic reaction barriers via the concerted path parallel those experimental rates observed for the disulfone

derivatives. There is an apparent correlation between the reaction barriers of sesquinorbornenes and the H-C(sp²) distances of the reactants, although these concerted transition structures except for norbornene have similar geometries of the reaction center and reaction barriers are lower than that of the intramolecular ethylene-ethane reaction. The nonconstrained intermolecular transition structure has a planar six-membered ring center, which is distorted to a boat conformation in the

Table 3. Results of *Ab initio* Calculations on the Intramolecular Dyotropic Hydrogen Transfer. Energies are Evaluated at the MP2/3-31G* Level Using the HF/3-21G Geometries (UHF for Open-Shell Species)

Compd	(Å) C _{sp²} -C _{sp³}	(Å) C _{sp²} -HC	ΔE [‡] (kcal/mol) MP2/6-31G* //HF/3-21G	ΔE radical MP2/6-31G* //HF/3-21G
	2.82	2.22	30.9	
	2.97	2.33	37.7	64.7
	3.01	2.38	39.9	65.2
	3.14	2.50	43.9	63.4
	3.66	3.08	47.9	
	----	----	50.8	67.8
	2.47	2.66	107.2	65.4
	3.02	2.41	39.2	

transition structures of the intramolecular reactions. This distortion increases the reaction barrier of intramolecular reactions to some extent, but it is well-compensated by a decrease of the reaction barrier due to the release of unfavorable nonbonding interactions of the reactant. However, when the transition structure of intramolecular double hydrogen transfer reaction is highly distorted as in the case of norbornene, the reaction barrier becomes much higher than in intermolecular reactions.

On the other hand, the calculated energy gap between the reactant and biradical intermediate was less sensitive to the structural variations and the steric strain of the reactant. As shown in Table 3, all the intramolecular reactions involve the biradical intermediate that are ~64 kcal/mol higher in energy than the reactant. The biradical intermediate of the intermolecular reaction (ethylene plus ethane) is 68 kcal/mol above the reactants at the same level of theory. The larger value of the latter can be accounted for by the lack of radical stabilization by alkyl groups. It seems that the same amount of energy is required for the formation of the biradical intermediates in the double hydrogen dyotropy regardless of ground state strain. Thus, the wide range of reaction rates could not be predicted simply upon the energies of the biradical intermediates.

The features of these *ab initio* transition structures (Figure 3) were considered in the development of transition state force fields. All of the intramolecular hydrogen transfer reactions

were found to have very similar transition structures in terms of bond lengths and bond angles associated with the forming and breaking bonds at the reaction centers. In particular, the C-H distance in the transition state structures varies little from the intermolecular ethylene-ethane reaction to the intramolecular reactions, and this may be considered the "critical distance" for these dyotropic reactions. The epoxide series is intrinsically less reactive than the other sesquinorbornadienes, suggesting that it costs more energy to distort the epoxide O-C-C than the exocyclic C-C-C bending of the cyclopropane ring.

Since the experimental rates observed for this series of molecules seem to follow the order of release of ground state strain,⁶ we calculated the strain of the ground and transition states using empirical force fields. For the ground state molecules, the existing MM3 force field developed by Allinger et al. was used.³² We then developed an MM3 force field for the concerted transition states of the dyotropic hydrogen transfer reactions in question using geometries derived from the *ab initio* 3-21G transition structures described later. This follows the general treatment for many organic reactions reported earlier where the MM2 force field was adopted.³³

The force field parameters were adjusted so that the calculated steric energy differences between the transition state and ground state correlate linearly with the natural log of the experimentally observed rates available at the time. We used the rates rather than the measured activation energies during the force field development based upon the following considerations. First, experimental rate constants were more plentiful than activation energies. Second, these reaction rates were shown experimentally not to be dominated by activation entropy.

A methyl group was initially used in place of the PhSO₂ during the force field modeling. The calculated rates were always found to be too low for compounds with substituents at the apical carbon near the phenyl sulfonyl groups. This indicated that the nonbonded steric repulsion between the sulfonyl group and groups at the close apical carbon influences the rate significantly, and a methyl group poorly represents the steric crowding of the PhSO₂ group. In the force-field modeling reported here, a methyl sulfonyl was used to better mimic the PhSO₂ group. The magnitudes of repulsion for groups at the apical carbon were found to follow the order of cyclopropyl, =C(CH₃)₂ > H. Similar nonbonded steric repulsion exists between groups at the apical carbon and the central methylene bridge in the cyclopropane compounds, but compounds with hydrogens at the apical carbon seemed to be more strained than those with cyclopropyl or =C(CH₃)₂ groups. This is also manifested in the *ab initio* structures where the axial methylene hydrogens are distorted both in the ground state and transition state of the cyclopropane derivative. Thus, groups at the apical carbon may introduce different steric and structural effects depending on the surrounding groups.

After the MM3 force field was developed, some predictions were made for rates of several compounds whose experimental measurements were under way. When the new experimental data became available, reasonable agreement was seen. Figure 7 shows a plot of log *k*_{rel} of experimental rate constants for hydrogen transfer versus the differences in activation energies calculated from the force field model. The calculations show that the relative rates of reaction are related to the energies required to distort the reactants to the transition state geometries.

The results do not prove that the reactions go through the concerted mechanism. The isotope effects reported here show

(32) Allinger, N. L.; Yuh, Y. H.; Lii, J.-H. *J. Am. Chem. Soc.* **1989**, *111*, 8551.

(33) Eksterowicz, J. D.; Houk, K. N. *Chem. Rev.* **1993**, *93*, 2439.

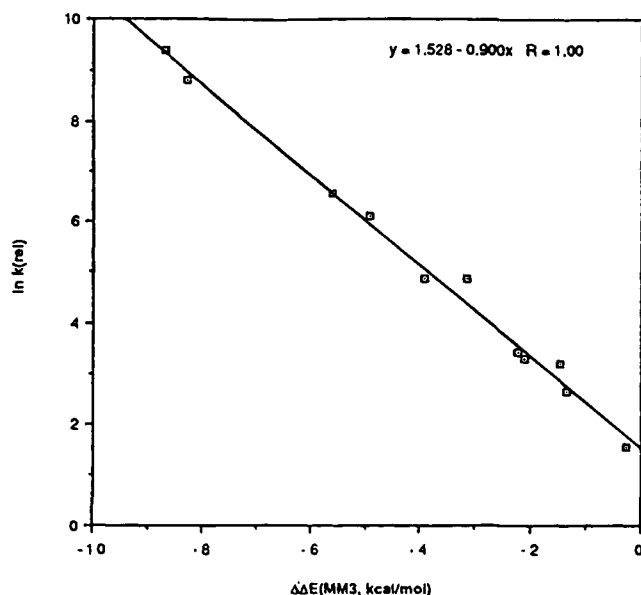


Figure 7. Plot of experimental $\ln k_{rel}$ for hydrogen transfer versus the differences in calculated activation energies by MM3.

that tunneling is significant in at least some of the cases investigated. Tunneling might occur at some geometry less distorted than the transition structure. A stepwise mechanism might also occur, with tunneling, and unsymmetrical distortion would be required to achieve the tunneling geometry. In the next section, both concerted and stepwise processes are investigated computationally at the multiconfigurational SCF (MCSCF) level of theory.

Potential Energy Paths for the Concerted and Stepwise Hydrogen Transfer. Assuming a concerted path, Frontera et al. reported a study on similar intramolecular reactions using the semiempirical MNDO and AM1 methods.³⁴ The stepwise path involving a biradical intermediate was not considered in their study, which would otherwise be predicted artificially too favorable by these methods. This is evident in the case of calculations on the reaction of ethylene with ethane reported by Agrafiotis and Rzepa.³⁵ The calculated heat of reaction for the formation of two ethyl radicals from ethane and ethylene is 2.5 kcal/mol by MNDO and 32 kcal/mol by AM1. These values are significantly less than the experimental value of 60 kcal/mol.³⁶ The stabilities of radical intermediates are overestimated to an extent greater than 28 kcal/mol by both MNDO and AM1 methods! On the other hand, the barrier calculated by MNDO is extraordinarily high (>80 kcal/mol) for the concerted synchronous mechanism.³⁵ In contrast to the semiempirical methods, *ab initio* calculations at the MP2/6-31G* level predict that double hydrogen transfer between ethane and ethylene has a barrier of 50 kcal/mol via the concerted path,⁹ two ethyl radicals are 18 kcal/mol higher in energy than the concerted transition structure.³⁶ However, these calculations are biased toward the closed-shell transition state. *Ab initio* MCSCF calculations treat the open-shell biradical species and the closed-shell transition structures in a balanced way, and such calculations were undertaken in order to achieve additional insights into the nature of potential energy paths of these dyotropic hydrogen transfer processes.

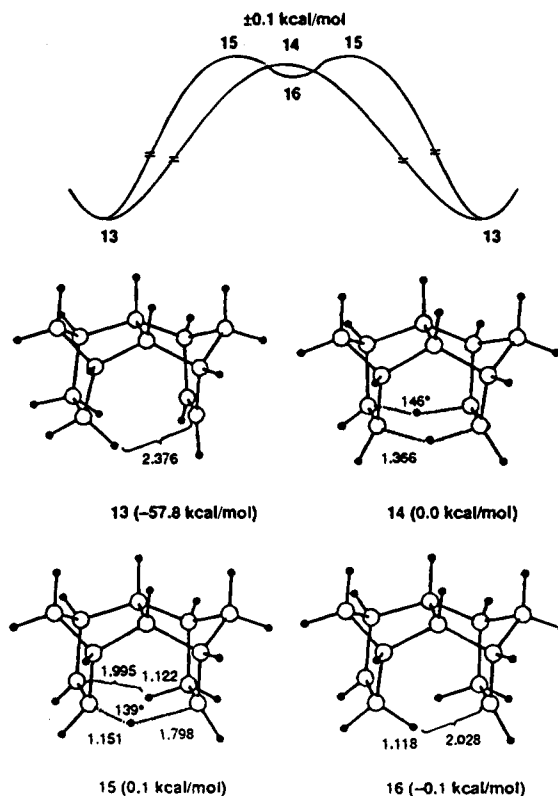


Figure 8. CASSCF (6e/6mo)/3-21G optimized structures and energies. Bond lengths are in angstroms, and bond angles are in degrees.

The multiconfiguration wave function in the MCSCF calculation consists of configuration state functions generated from a complete active space³⁷ involving six electrons in six orbitals. The six active orbitals correspond to the π and π^* orbitals of the alkene and the σ and σ^* orbitals of the two C-H bonds broken during the double hydrogen transfer reaction. The choice of the active space is based upon chemical intuition as to the orbitals involved in bonding changes taking place during the reaction, although a similar active space would have been chosen based upon Pulay's approach³⁸ using the unrestricted HF (UHF) natural orbital population analysis of the concerted transition structure. At this complete active space SCF (CASSCF) level of theory,³⁷ STO-3G and 3-21G basis sets³⁰ were used, and geometries were fully optimized within the proper symmetry constraints using Baker's gradient method.³⁹ The transition structures and the biradical intermediate located at the CASSCF/STO-3G level were further verified by vibrational frequency analysis using numerically calculated secondary derivatives. All MCSCF calculations were carried out using the GAMESS program.⁴⁰

Figure 8 shows the optimized geometries and relative energies of reactant sesquinorbornene **13**, the transition structure **14** for the concerted hydrogen transfer, the transition structure **15** for the stepwise hydrogen transfer leading to a biradical intermediate, and the biradical intermediate **16**. The transition structure for the concerted path has C_{2v} symmetry and is thus synchro-

(37) (a) Roos, B. O. In *Adv. Chem. Phys.* Lawley, K. P., Ed.; Wiley-Interscience: New York, 1987; pp 339. Roos, B. O. *Int. J. Quantum Chem. Symp.* **1980**, *14*, 175.

(38) Pulay, P.; Hamilton, T. P. *J. Chem. Phys.* **1988**, *88*, 4926. (b) Tu, H.; Goddard, J. D. *J. Mol. Struct. (THEOCHEM)* **1991**, *223*, 129.

(39) Baker, J. *J. Comput. Chem.* **1986**, *7*, 385.

(40) (a) Dupuis, M.; Spangler, D.; Wendoloski, J. J. *GAMESS*, Program QC01, National Resource for Computations in Chemistry Software Catalog, University of California, Berkeley, CA, 1980. (b) Schmidt, M. W.; Baldridge, K. K.; Boatz, J. A.; Jensen, J. H.; Koseki, S.; Gordon, M. S.; Nguyen, K. A.; Windus, T. L.; Elbert S. T. *QCPE Bull.* **1990**, *10*, 52.

(34) Frontera et al. *J. Org. Chem.* **1992**, *57*, 6731.

(35) (a) Agrafiotis, D. K.; Rzepa, H. S. *J. Chem. Soc., Perkin Trans. 2* **1989**, 475. (b) Agrafiotis, D. K.; Rzepa, H. S. *J. Chem. Soc., Chem. Commun.* **1987**, 902.

(36) Benson, S. W. *Thermochemical Kinetics*; Wiley-Interscience: New York, 1976.

nous, involving equal breaking and forming C–H bond lengths of 1.37 Å. In contrast, transition structure **15** of the stepwise path leading to the biradical intermediate is highly asynchronous; one of the transferring hydrogens has almost completed the transfer while migration of the other hydrogen lags far behind. The breaking C–H bond length is 1.80 Å while the forming bond length is 1.15 Å. In fact, this transition structure **15** has essentially the same geometry as biradical intermediate **16**, as expected from the Hammond postulate.⁴¹ Simple UHF calculations predicted a less asynchronous transition structure in which the breaking and forming C–H bond lengths are 1.47 and 1.24 Å, respectively. Among all the structures shown in Figure 8, the concerted transition structure has the most compressed sesquinorbornene carbon skeleton. It is interesting that the distance between the second transferring hydrogen and the radical carbon center in **16** is 0.35 Å shorter than the corresponding distance in the reactant. It is unlikely that there are attractive interactions between the radical center and the transferring hydrogen in the biradical intermediate. At most, this indicates that the carbon radical centers repel hydrogens in the close proximity less than the sp² carbons in the reactant. There is a very small barrier from the biradical intermediate to the product. This barrier disappears after zero-point energy corrections.

MCSCF calculations thus predict that the energy barrier via the concerted mechanism is identical to that involving a stepwise mechanism for the intramolecular double hydrogen transfer in sesquinorbornene **13**. Although MCSCF calculations take nondynamic electron correlation into account, dynamic electron correlation energy corrections are limited in these calculations. McKee showed that the inclusion of dynamic correlation energy corrections dramatically lowers the barrier for the concerted path of double hydrogen transfer in the ethylene–ethane reaction.⁹ The barrier via the stepwise biradical mechanism is expected to be less sensitive to the dynamic correlation. By comparison, calculations on **13** using semiempirical theory with the PM3 Hamiltonian revealed that the stepwise mechanism is strongly preferred. That is, the transition state (**14**) for the concerted mechanism is 37.7 kcal/mol higher in energy than **13**; while **15**, the transition state for formation of biradical **16**, is only 28.4 kcal/mol higher in energy than **13**. Biradical **16** is calculated to be 5.7 kcal/mol below **15**. Clearly, the PM3 generated surface is qualitatively different than the *ab initio* surface, and these results reflect the general tendency of semiempirical methods to overestimate the stability of biradicals.

For comparison to those calculations, the intermolecular dyotropic hydrogen transfer between ethane and ethylene was calculated at the same CASSCF/3-21G level of theory. At this level, the concerted transition structure is 0.8 kcal/mol higher in energy than two ethyl radicals. The concerted transition structure is 14.9 kcal/mol lower in energy than ethyl radicals when calculated at the QCISD(T)/6-311G* level including high-level dynamic electron correlation energy corrections. Inclusion of dynamic electron correlations has a more significant effect upon the concerted path than on the stepwise biradicals and should substantially lower the barrier involving the concerted transition structure. Thus, for the intramolecular double hydrogen transfer in **13**, the concerted path is predicted to be more favorable than the stepwise pathway.

The calculations suggest that the potential surface for the dyotropic shift is rather flat, with the possibility of both stepwise and concerted mechanisms. Furthermore, the concerted mechanism may be highly asynchronous, or synchronous, or anything in between. This situation is best illustrated by a contour

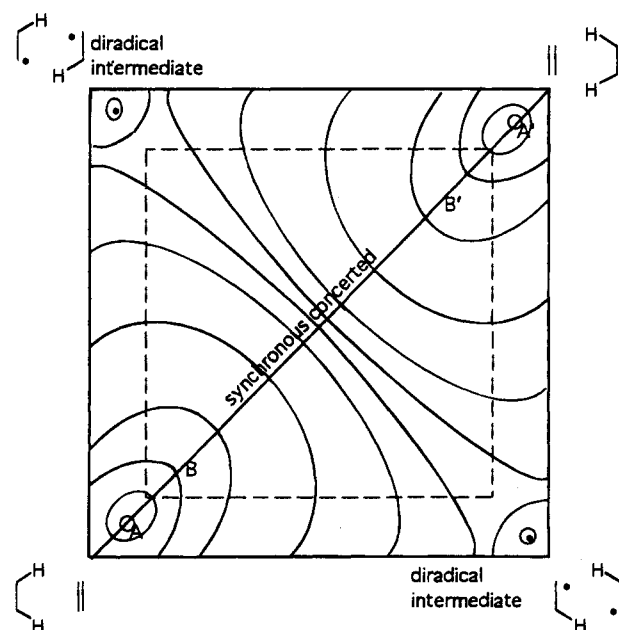


Figure 9. Contour diagram for a dyotropic hydrogen shifts. The outer boundaries represent the situation when the migration origins and termini are held apart by a relatively rigid molecular skeleton; the positions marked A and A' represent reactant and product minima. The dashed boundary represents the situation where the two fragments may come close together due to a flexible framework. Point B and B' indicate minima of molecules which have the origin and termini closer to each other.

diagram as shown in Figure 9 for the double hydrogen transfer between ethylene and ethane. This More O'Ferrall-Jencks type diagram shows idealized contours for various reaction paths. The diagonal pathway represents the synchronous pathway, where the transfers of the two hydrogens from A to A' are coupled. Travel along one horizontal or vertical axis corresponds to motion (*i.e.* transfer) of one hydrogen at a time. In calculations on **13**, this leads to a very shallow diradical intermediate. However, if the carbon skeleton were more rigid, or if the two C₂ groups were held apart in some other way, there could be a deeper energy minimum for the diradical intermediates at the lower right or upper left corners of the diagram. In such cases, the concerted pathway will be disfavored, and the activation energy for the hydrogen transfer will increase as the distance between the heavy atom termini increases.

If the skeleton is flexible, or if the ethane and ethylene units are held close to each other, the hydrogen transfer reaction will have the alternate limits represented by the dashed lines in Figure 9. Points B and B' on the curves will now represent the energy minima for reactants and products. The diradical will not be stable if the two fragments are allowed to come in close proximity to each other. In such a case, the mechanism may vary from concerted synchronous to concerted asynchronous, with the former preferred when the approach of the ethane and ethylene fragments is facilitated.

One-Dimensional Barrier Treatment. To relate the observed rate constants to the quantum-chemical calculations, a dynamical model is required. In earlier quantum-chemical model studies,^{8,9} the calculated barrier height for concerted transfer was compared directly to the observed activation energy of the transfer. However, this is not justified because the transfer involves light atoms capable of quantum-mechanical tunneling through potential-energy barriers. It is well-known that the corresponding rate constants do not follow the Arrhenius equation: their semilog plot against the inverse absolute

(41) Hammond, G. S. *J. Am. Chem. Soc.* **1955**, *77*, 334.

Table 4. Comparison of Calculated and Observed^a Rate Constants for Double Hydrogen Dyotropy in **3a**, **4a**, and **5a** for an Asymmetric Eckart Barrier^b with Adjustable Height^c and an Asymmetry Equal to the Observed Exothermicity^d

compd	log k_{calc} (373 K)	log k_{obs} (373 K)	log k_{calc} (403 K)	log k_{obs} (403 K)
3a	-4.31	-4.30	-2.99	-3.16
4a	-4.83	-4.69	-3.46	-3.44
5a	-5.26	-5.39	-3.86	-3.94

^a See Table 1. ^b Tunneling distance $L = 1.52 \text{ \AA}$, isotopic masses of 2, 3, and 4 for **3a**, **4a**, and **5a**, respectively. ^c The rate constants listed correspond to an adjusted barrier height of 32.2 kcal/mol for **3a** with zero-point corrections for **4a** and **5a**. ^d 1 kcal/mol.

temperature yields a curve rather than a straight line, so that the slope varies with temperature and cannot be equated with the barrier height.^{12a}

The simplest available treatment of transport involving tunneling is based on a model in which a particle with a kinetic energy equal to the thermal energy $k_B T$ penetrates a one-dimensional barrier. For concerted transfer in our systems, the mass of this particle in atomic mass units would be 2, 3, or 4 for HH, HD, or DD transfer, respectively. The barrier is usually represented by a convenient analytical function. Although this model does not explicitly consider vibrations, ad hoc corrections of the barrier height for zero-point energy differences are introduced occasionally; this has the effect of increasing the barrier slightly with increasing isotopic mass of the particle. Since for the present systems the tunneling distance and the exothermicity are known experimentally, only one additional parameter is required to construct a simple analytical barrier, namely the barrier height. In principle, it could be represented by the calculated height; however, it is more practical to use it as an adjustable parameter and fit it to the data in order to obtain an "observed" barrier height that can be compared with the quantum-chemical calculations.

Of the various simple analytical barriers proposed, the Eckart barrier is probably the most satisfactory.^{12a} It is defined by

$$V(x) = (Az + B)(1 - z); \quad z^{-1} = 1 + \exp(2\pi x/L)$$

where x is the reaction coordinate, $2L$ is the effective tunneling distance, B determines the asymmetry of the barrier, and A is related to the barrier height through

$$V_0 = (A + B)^2/4A$$

For a particle of mass m , the permeability of the barrier is given by^{12a}

$$G(E) = \frac{\sinh^2[1/2pL(1 + \Delta)] - \sinh^2[1/2pL(1 - \Delta)]}{\sinh^2[1/2pL(1 + \Delta)] + \cosh^2[(2mL^2A - \pi^2\hbar^2)^{1/2}/2\hbar]}$$

where $p = (2mE)^{1/2}$ and $\Delta = (1 - B/E)^{1/2}$. The transfer rate constant will then be

$$k = (C/k_B T) \int_0^E G(E) \exp(-E/k_B T) dE$$

where the pre-exponential factor C is set equal to the frequency of the symmetric C-H or C-D stretching mode (10^{14} s^{-1} or $7 \times 10^{13} \text{ s}^{-1}$).

Typical results of these calculations are listed in Table 4. The calculated rate constants are fairly close to the observed rate constants and the observed temperature and isotope effects are reasonably well reproduced for a barrier height of 32.2 kcal/mol. Although this value is considerably smaller than the

calculated barrier height, the one-dimensional barrier model is best regarded as a semiempirical scheme in which the parameters need not be directly comparable with actual physical parameters.¹¹

Similar calculations have been carried out for asynchronous transfer, involving an assumed metastable intermediate state. The corresponding single atom transfer is highly endothermic so that the appropriate Eckart potential will be strongly asymmetric. With both A and B adjustable, it is possible to obtain a somewhat more accurate fit to the data than for synchronous transfer, but because of the extra adjustable parameter, this is not assumed to be significant. Actually, an acceptable fit can be obtained for a range of A and B values, so that these parameters cannot be determined accurately on the basis of kinetic data. A barrier of about 32 kcal/mol, as obtained above for synchronous tunneling, would give rise to an intermediate state energy of about 22 kcal/mol, very much lower than calculated.

It follows that the Eckart-barrier model cannot discriminate between the two transfer mechanisms on the basis of the available kinetic data, due to the very limited temperature range for which such data are available. In the case of porphyrins, discrimination was possible because another kinetic window was available⁴² which allowed measurement of the rate constants corresponding to NMR frequencies. In the absence of such data, other information is needed before a clear choice can be made. One piece of information is the form of the barrier calculated quantum-chemically which clearly favors a barrier without a stable intermediate.

Obviously, a one-dimensional barrier approach is very primitive and unlikely to yield results that are quantitatively accurate for our complex molecules. In the next section, we therefore reexamine the transfer dynamics in terms of a more elaborate model that has proved reasonably accurate in the case of porphine.

Two-Dimensional Barrier Treatment. In principle, a much more precise description of a tunneling reaction is obtained if the vibrational modes involved in the transfer are considered explicitly. In particular, a separate treatment of the modes of the tunneling hydrogen atom and of the other modes would seem to be instructive. Among the available treatments, we choose the Golden Rule approach and follow the procedure recently applied to the intramolecular exchange of the two inner hydrogen atoms in free-base porphyrins.¹⁶ In this treatment, the hydrogen bending and stretching modes are treated separately from the skeletal modes. On the basis of calculated vibrational force fields, the latter modes are reduced to a single effective mode reflecting the properties of the low-frequency modes that have a strong effect on the tunneling distance. As a result of these skeletal vibrations, the tunneling barrier oscillates with the frequency of the effective mode whose amplitude increases with the degree of excitation. The rate constant is expressed in terms of the Golden Rule and is governed by the vibrational overlap (Franck-Condon) factors between the initial and the final state of the transfer. In the simplest version of the model this overlap integral is written as the product of the overlap integrals of the hydrogenic and the skeletal modes so that the model is effectively two-dimensional.

A characteristic property of the model is that a rise in temperature affects the tunneling rate mostly through the increased population of excited levels of the low-frequency mode, since their population increases much more rapidly with temperature than those of the hydrogenic mode. This provides a very effective mechanism for increasing the rate of tunneling;

this increase is thus due to the increased oscillation of the barrier rather than the increased kinetic energy of the tunneling atom. As a result, the "activation energy" of a tunneling reaction, which typically is constant only over a narrow temperature range, tends to be lower than the calculated barrier height.

The tunneling rate is calculated by means of the Golden Rule as a rate of transfer from an initial state $|i\rangle$ to a final state $|f\rangle$ under the influence of a perturbation ("coupling") J and subject to energy conservation:¹¹

$$k = (2\pi/\hbar) |\langle f|J|i\rangle|^2 \delta(\epsilon_f - \epsilon_i)$$

The initial and final states are products of vibrational wave functions of the reactants and reaction products, respectively, and the coupling J is an electronic integral over the carbon orbitals involved in the reacting CH bonds. Temperature dependence is introduced by summing over the vibrational state populations. The vibrational eigenfunctions are separated into CH modes and framework modes. The rate of tunneling is governed by the overlap of the CH wave functions in the reactants and products and this overlap will strongly depend on the displacement (tunneling distance, $2L$) of the hydrogen atom. The distance oscillates with the frequencies of the framework modes so that the overlap integral should be integrated over the framework vibrations.

To implement this program in detail, information is required that is not available for the molecules under consideration. We therefore introduce a number of simplifications. In view of the relatively high temperatures used to obtain the rate constants, we treat the framework modes classically and write⁴³⁻⁴⁵

$$k(T) = \int k(R)p(R) dR$$

where $p(R)$ is a function representing the distribution of distances R between the donor and acceptor carbon atoms which for an harmonic oscillator takes the form⁴⁶

$$p(r) = [2\pi/A^2(T)]^{-1/2} \exp[-(R - R_0)^2/A^2(T)]$$

R_0 being the equilibrium value and $A^2(T)$ the mean square amplitude of R . Following an earlier analysis,⁴⁷ we represent the framework by a single effective mode of frequency Ω and reduced mass M , so that

$$A^2(T) = (\hbar/M\omega) \coth(\hbar\Omega/2k_B T)$$

We also use an effective mode for the hydrogen vibration, taking into account that the CH bond makes an angle of about 38° with the line connecting the donor and acceptor carbons. For the frequency of this mode we take¹¹

$$\omega^H = \omega_{\text{stretch}}^H \cos^2 38 + \omega_{\text{bend}}^H \sin^2 38 \cong 2500 \text{ cm}^{-1}$$

We represent these vibrations by Morse oscillators with anharmonicities⁴⁸ $X^H = 55 \text{ cm}^{-1}$, $X^D = X^{2H} = 28 \text{ cm}^{-1}$, and $X^{2D} = 14 \text{ cm}^{-1}$. The reduced masses are $M^H = 1$, $M^{2H} = M^D = 2$, $M^{2D} = 4$ and the CH bond length is taken to be $L_0 = 1.08 \text{ \AA}$. These values allow us to calculate the CH vibrational overlap

(43) Benderskii, V. A.; Goldanskii, V. I.; Ovchinnikov, A. A. *Chem. Phys. Lett.* **1980**, *73*, 492.

(44) Egorev, V. V. *Z. Fiz. Khimii* **1980**, *73*, 492.

(45) Smedarchina, Z. *Khimicheskaya Fizika* **1992**, *11*, 883

(46) Maradudin, A. A.; Montroll, E. W.; Weiss, G. H.; Ipatova, I. P. *Theory of Lattice Dynamics in the Harmonic Approximation*; Academic Press: New York, 1971; p 307.

(47) Smedarchina, Z. *Chem. Phys.* **1991**, *47*, 150. Smedarchina, Z.; Siebrand, W.; Zerbetto, F. *Chem. Phys.* **1993**, *170*, 347.

(48) Gough, K. M.; Henry, B. R. *J. Phys. Chem.* **1984**, *88*, 1298.

integrals as a function of tunneling distance for vibrational quantum states ν_i and $\nu_f = \nu_i + \Delta E/\omega$ where ΔE is the exothermicity of the reaction. Since ω is large compared to $k_B T$, it is found that only the lowest quantum numbers make a sizeable contribution so that, depending on ΔE , either ν_i or ν_f can be taken to be zero. The tunneling rate constant for fixed R is then given by

$$k(R) = (2\pi/\hbar) \Lambda(J) |S_{0\nu}(R)|^2 / \hbar \Omega$$

where S is the overlap integral, $1/\hbar\Omega$ is the density of states which, as usual,¹¹ replaces the δ function in eq 1, and the factor $\Lambda(J)$ replaces the standard weak coupling factor J^2 in the case of strong and intermediate coupling ($J \geq \hbar\omega$).¹⁶ The exothermicity takes two different forms. For synchronous tunneling, it is an experimentally measured quantity which we represent by δE ; we thus have $\nu_i = 0$ and $\nu_f = \delta E/\hbar\omega$. For asynchronous tunneling, there are two steps: for the first step we have $\nu_i^{(1)} = \Delta E/\hbar\omega$ and $\nu_f^{(1)} = 0$, for the second step, $\nu_i^{(2)} = 0$, and $\nu_f^{(2)} = (\Delta E + \delta E)/\hbar\omega$. Although ΔE is not known a priori, it should be close to the observed activation energy.

For the mixed (HD) isotopes, there are two contributions to asynchronous transfer, depending on which atom transfers first. Both are included in the calculations. It is not immediately clear how to handle synchronous tunneling for mixed isotopes since the two tunneling atoms vibrate with different frequencies so that they will move synchronously only for a time shorter than the vibrational period and thus also much shorter than the time required to tunnel through the barrier. Since the corresponding relative inefficiency of mixed transfer was not observed experimentally, we have made no attempt to develop a model for synchronous tunneling of particles of different mass.

Our fitting procedure starts with the asynchronous mechanism. To reduce the number of adjustable parameters, we assume initially that the same parameter values apply to both molecules **3a-5a** and **3b-5b**, except for the tunneling distance $2L$ and the exothermicity for which we take the experimental values, and the energy of the intermediate states, which we assume to differ by the same amount as the observed activation energies. For the reduced mass of the effective framework mode, we adopt a value of 40. This leaves us with three adjustable parameters, Ω , J , and ΔE to calculate six rate constants and their temperature dependences. In this manner it is possible to obtain a satisfactory fit to the data for reasonable parameter values. The introduction of two physically reasonable refinements allows us to obtain a very good fit: (i) we allow J to be smaller for the molecule with the larger tunneling distance,¹¹ and (ii) we allow a slightly higher CH anharmonicity in the products compared to the reactants in view of the expected effect of the sulfone group on the CH bond energy. The final parameter values are listed in Table 5, and the corresponding fit is illustrated in Figures 10 and 11.

Now we turn to the synchronous mechanism, using the same trial-and-error method to try fitting the data. It emerges that no set of parameter values can be found that fit the data even approximately. If the parameters are adjusted to fit one rate constant at one temperature, the model becomes inappropriate for other temperatures and other isotopic masses. Specifically, the predicted temperature dependence is much too low and the predicted isotope effect much too high. A typical result is illustrated in Figure 12. The cause of this failure is the efficiency with which the low-frequency mode promotes tunneling when it becomes vibrationally excited. As a result, the hydrogens tunnel well below the top of the barrier: hence the underestimation of the temperature effect and the overestimation of the isotope effect. In the case of asynchronous tunneling,

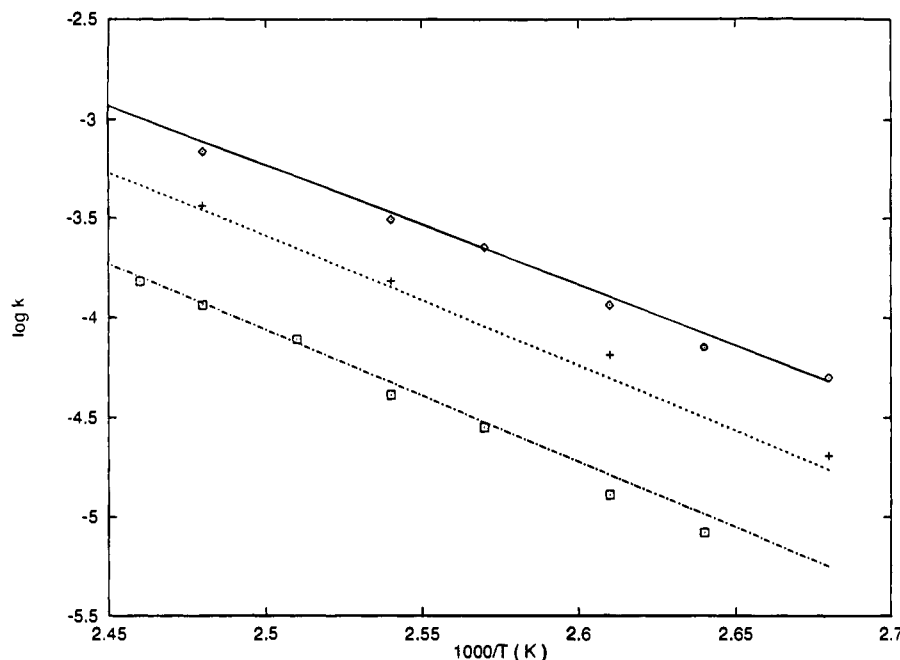


Figure 10. Comparison of the observed rate constants for **3a** (top), **4a** (center), and **5a** (bottom) with theoretical curves calculated for asynchronous tunneling through a two-dimensional barrier characterized by the parameter values listed in Table 5.

Table 5. Model Parameters Used To Calculate the Rate Constants for Synchronous and Asynchronous HH, HD, and DD Transfer Displayed in Figures 9–11

parameter values	compounds 3a–5a		compounds 3b–5b
	asynchronous mechanism	synchronous mechanism	asynchronous mechanism
ΔE , kJ/mol	90	4	79.5
δE , kJ/mol	4		12.5
$m_{\text{H/D}}$, amu	1/2	2/4	1/2
$\omega_{\text{H/D}}$, cm^{-1}	2500/1850	2500/1850	2500/1850
$X_{\text{H/D}}^{\ddagger}$, cm^{-1}	55/28	27/14	55/28
$X_{\text{H/D}}^{\ddagger}$, cm^{-1}	60/32.5	30/16	60/32.5
$2L$, Å	1.52	1.52	1.48
L_0 , Å	1.08	1.08	1.08
Ω , cm^{-1}	95	118	95
m , amu	40	40	40
J , eV	0.220	0.220	0.219

the metastable intermediate dictates a level of tunneling much closer to the top of the barrier which eliminates these difficulties.

Modification of the model so as to favor the synchronous mechanism might include increasing the frequency of the low-frequency mode or making this mode anharmonic due to steric repulsion. We estimate, however, that the effect of such modifications is much too weak to change the conclusions. Hence we conclude that the two-dimensional barrier model clearly favors an interpretation of the data in terms of asynchronous or stepwise tunneling, assisted by a low-frequency twisting or bending mode of about 100 cm^{-1} .

Although it would be unjustified to claim that the values of the parameters obtained in the fitting are unique, they do seem reasonable. The low effective frequency $\Omega_{\text{as}} = 95 \text{ cm}^{-1}$ suggests that twisting of the framework is the most efficient way of promoting tunneling, an observation supported by elementary considerations of molecular mechanics. For synchronous transfer, asymmetric twisting will not help; the only framework modes that can effectively promote this transfer are symmetric bending modes, with frequencies expected to be higher than the twisting frequencies promoting asynchronous transfer. The observation that the latter transfer dominates in the temperature range investigated sets a lower limit ($\Omega_{\text{s}} \geq 118$

cm^{-1}) to the effective bending mode frequency corresponding to the parameter values of Table 5.

Direct Dynamics Calculations

Since hydrogen transfer reaction rates are typically dominated by quantum mechanical tunneling,⁴⁹ it is not unreasonable to expect that such tunneling will play an important role in the mechanism of double hydrogen dyotropy in *syn*-sesquinorbornenes. It is also conceivable that variational effects could cause the adiabatic free energy maximum (transition state) to be shifted away from the maximum (TS) on the electronic structure calculated potential energy surface (PES).⁵⁰ To explore the significance of these two effects, and to further probe the mechanism of double hydrogen dyotropy in *syn*-sesquinorbornenes, model systems were studied with direct dynamics methods as developed by Truhlar *et al.*⁵¹ and implemented in the program MORATE.^{51a}

MORATE (molecular orbital rate calculations) is a computer program for direct dynamics calculations of gas-phase chemical reaction rates, using semiempirical molecular orbital theory to represent the potential energy of interaction. This is similar to POLYRATE, also written by Truhlar *et al.*^{51b} which has successfully been used for direct dynamic calculations on a

(49) (a) Truhlar, D. G.; Garrett, B. C. *J. Am. Chem. Soc.* **1989**, *111*, 1232. (b) Bell, R. P. *The Proton in Chemistry*, 2nd ed.; Chapman and Hall: London, 1973; Chapter 12. (c) Melander, L.; Saunders, W. H., Jr. *Reaction Rates of Isotopic Molecules*, 2nd ed.; John Wiley & Sons: New York, 1980.

(50) (a) Truhlar, D. G.; Isaacson, A. D.; Garrett, B. C. In *The Theory of Chemical Reaction Dynamics*; Baer, M., Ed.; CRC Press: Boca Raton, FL, 1985, Vol. 4. (b) Garrett, B. C.; Truhlar, D. G. *J. Am. Chem. Soc.* **1979**, *101*, 4534. (c) Isaacson, A. D.; Truhlar, D. G. *J. Chem. Phys.* **1982**, *76*, 1380.

(51) (a) Lynch, G. C.; Liu, Y.-P.; Hu, W.-P.; Melissas, V. S.; Truong, T. N.; Lu, D.-h.; Stewart, J. P. P.; Barrett, B. C.; Steckler, R.; Isaacson, A. D.; Gonzalez-Lafont, A.; Rai, S. N.; Hancock, G. C.; Joseph, T.; Truhlar, D. G. MORATE-version 5.0, University of Minnesota, Minneapolis, MN, 1993. (b) Lynch, G. C.; Liu, Y.-P.; Hu, W.-P.; Melissas, V. S.; Truong, T. N.; Lu, D.-h.; Garrett, B. C.; Steckler, R.; Isaacson, A. D.; Rai, S. N.; Hancock, G. C.; Joseph, T.; Truhlar, D. G. POLYRATE, QCPE program 601-version 5.0.1, Quantum Chemistry Program Exchange, Indiana University, Bloomington, IN, 1993; *QCPE Bull.* **1993**, *13*, 28–29.

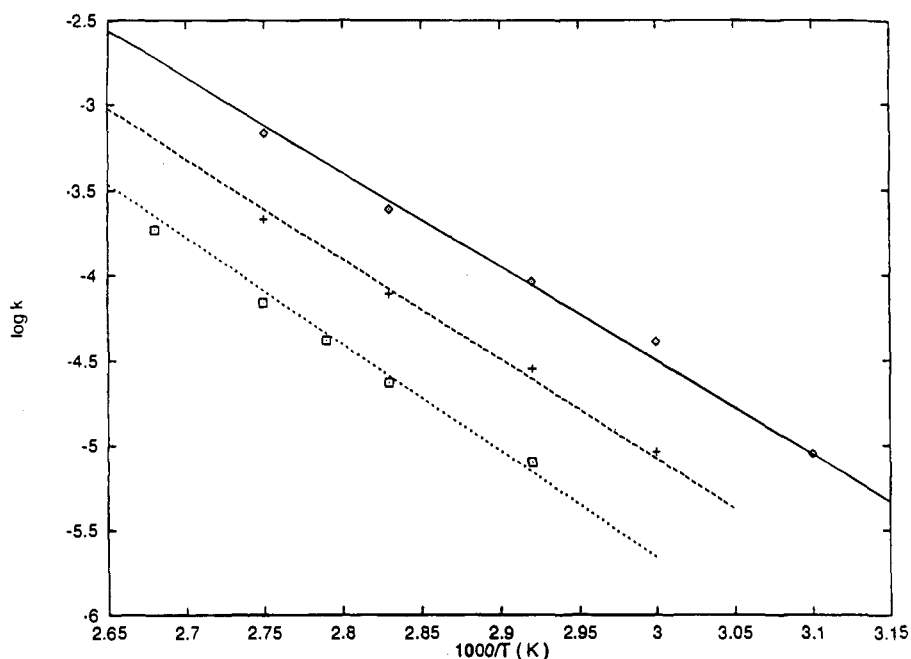


Figure 11. Comparison of the observed rate constants for **3b** (top), **4b** (center), and **5b** (bottom) with theoretical curves calculated for asynchronous tunneling through a two-dimensional barrier characterized by the parameter values listed in Table 5.

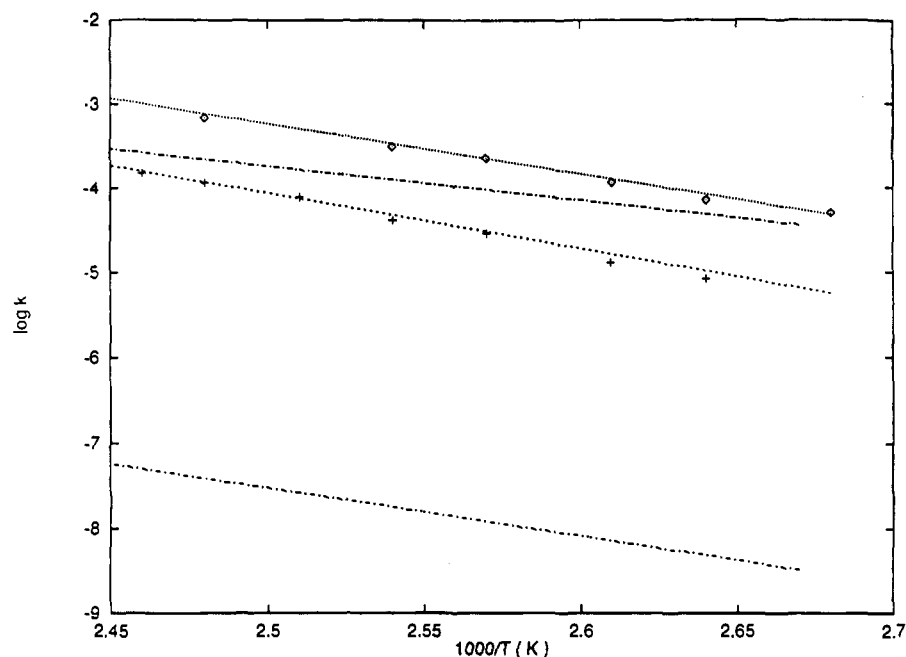
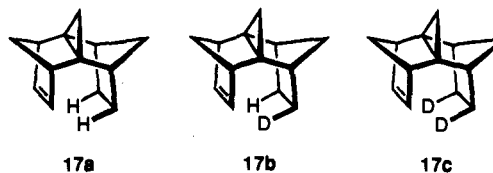


Figure 12. Comparison of the predictions of the two-dimensional barrier model for asynchronous (dotted curves) and synchronous (dot-dash curves) tunneling for **3a** (top) and **5a** (bottom). The parameter values are listed in Table 5.

variety of gas-phase reactions.⁵⁰ The primary difference between POLYRATE and MORATE is the choice of method used to describe the potential energy surface for the reaction under study. POLYRATE requires a user-supplied analytical or *ab initio* calculated potential energy surface, whereas MORATE is interfaced directly with MOPAC which supplies the potential energy of interaction (calculated using semiempirical molecular orbital theory) at any given point or trajectory on the reaction surface.

MORATE was used to calculate reaction rate constants for both the concerted (upper part of Figure 13) and stepwise (lower part of Figure 13) mechanisms for the double hydrogen transfer reaction of **17**. Compound **17** ($C_{13}H_{16}$) is a model compound which is identical to one of those used experimentally (**3a–5a**)

except **17** is lacking the SO_2Ph functionalities, which have been replaced by H for the purposes of computational economy.



Geometries, energies, gradients, and vibrational frequencies for all species along the various minimum energy reaction paths (MEP's) were generated using semiempirical theory as contained

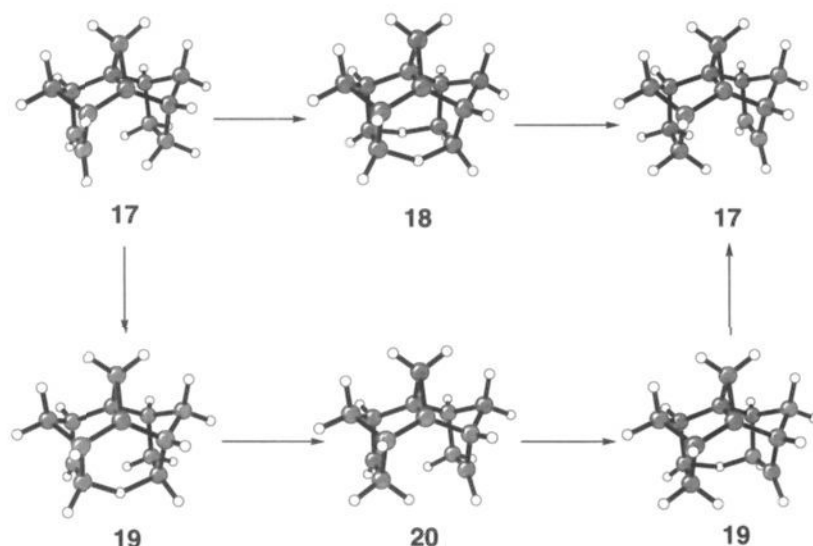
Figure 13. PM3 generated structures for $C_{13}H_{16}$ species.

Table 6. Summary of Calculated Rate Constants for 17a Concerted Double Hydrogen Transfer

T (K)	calculated rate constants (k_1) (s^{-1})			
	TST	CVT	TST/CD-SCSAG	CVT/CD-SCSAG
173.00	6.5996×10^{-32}	6.5182×10^{-32}	4.7406×10^{-15}	4.7115×10^{-15}
223.00	4.0156×10^{-22}	3.9583×10^{-22}	8.8721×10^{-13}	8.7846×10^{-13}
273.00	6.3617×10^{-16}	6.2574×10^{-16}	1.6615×10^{-10}	1.6396×10^{-10}
298.00	1.3306×10^{-13}	1.3074×10^{-13}	1.8419×10^{-9}	1.8149×10^{-9}
323.00	1.2193×10^{-11}	1.1969×10^{-11}	1.8084×10^{-8}	1.7993×10^{-8}
373.00	1.6747×10^{-8}	1.6409×10^{-8}	1.3255×10^{-6}	1.3009×10^{-6}
383.00	5.6714×10^{-8}	5.5550×10^{-8}	3.0113×10^{-6}	2.9542×10^{-6}
393.00	1.8058×10^{-7}	1.7681×10^{-7}	6.7482×10^{-6}	6.6174×10^{-6}
403.00	5.4307×10^{-7}	5.3157×10^{-7}	1.4902×10^{-5}	1.4606×10^{-5}
423.00	4.2068×10^{-6}	4.1151×10^{-6}	6.9224×10^{-5}	6.7797×10^{-5}
473.00	3.3164×10^{-4}	3.2394×10^{-4}	2.3394×10^{-3}	2.2870×10^{-3}
573.00	2.1487×10^{-1}	2.0937×10^{-1}	6.7290×10^{-1}	6.5587×10^{-1}

Table 7. Summary of Calculated Rate Constants for 17a Stepwise Double Hydrogen Transfer

T (K)	calculated rate constants (k_1) (s^{-1})			
	TST	CVT	TST/CD-SCSAG	CVT/CD-SCSAG
173.00	7.1513×10^{-18}	7.0944×10^{-18}	4.0122×10^{-15}	4.0146×10^{-15}
223.00	3.5943×10^{-11}	3.5751×10^{-11}	2.3133×10^{-9}	2.3159×10^{-9}
273.00	6.5336×10^{-7}	6.5102×10^{-7}	1.2202×10^{-5}	1.2207×10^{-5}
298.00	2.5895×10^{-5}	2.5820×10^{-5}	3.1599×10^{-4}	3.1650×10^{-4}
323.00	5.8406×10^{-4}	5.8271×10^{-4}	5.0684×10^{-3}	5.0770×10^{-3}
373.00	8.6126×10^{-2}	8.6010×10^{-2}	4.5112×10^{-1}	4.5199×10^{-1}
383.00	2.0039×10^{-1}	2.0013×10^{-1}	9.6931×10^{-1}	9.7094×10^{-1}
393.00	4.4696×10^{-1}	4.4668×10^{-1}	2.0071	2.0116
403.00	9.5863×10^{-1}	9.5814×10^{-1}	4.0168	4.0253
423.00	3.9649	3.9636	$1.4660 \times 10^{+1}$	$1.4687 \times 10^{+1}$
473.00	$8.2347 \times 10^{+1}$	$8.2342 \times 10^{+1}$	$2.3709 \times 10^{+2}$	$2.3729 \times 10^{+2}$
573.00	$7.4815 \times 10^{+3}$	$7.4809 \times 10^{+3}$	$1.5543 \times 10^{+4}$	$1.5527 \times 10^{+4}$

in MOPAC with the PM3 Hamiltonian.⁵² The intrinsic reaction path about each transition state was computed using the Euler single-step method⁵³ and with approximation of harmonic vibrations. These data were then used with either conventional (TST) or variational transition state theory⁵⁰ (VTST) to calculate rate constants and isotope effects for both the concerted and stepwise reactions depicted in Figure 13.

The rate constants are given in Tables 6–8 and in Tables IX–XV of the supplementary material. The VTST rate constants were generated using canonical variational theory

(52) Stewart, J. P. P., MOPAC-version 5.04, contained within MORATE-version 5.0, as in ref 51.

(53) Garrett, B. C.; Redmon, M. J.; Steckler, R.; Truhlar, D. G.; Gordon, M. S.; Baldrige, K. K.; Bartol, D. *J. Phys. Chem.* **1988**, *92*, 1476.

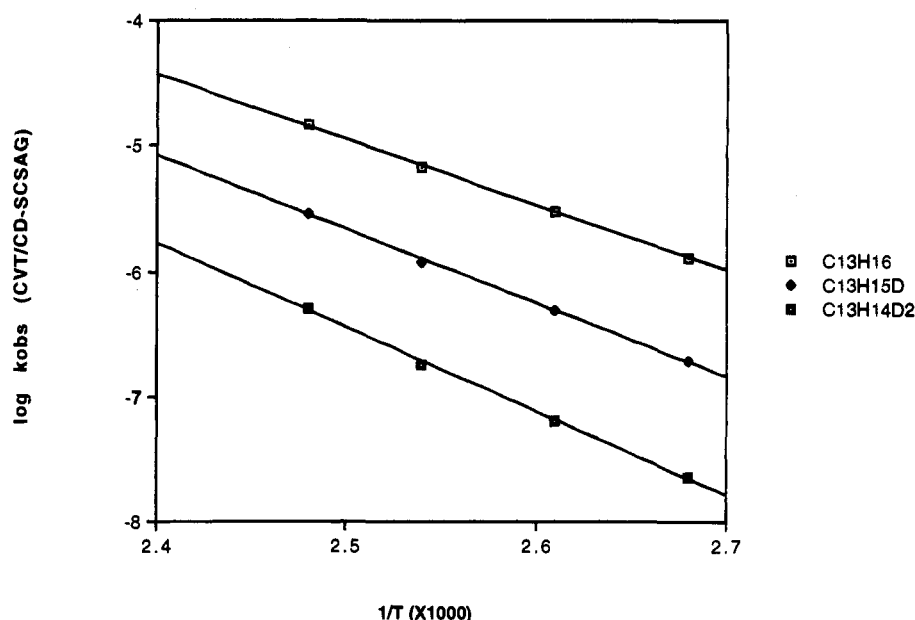
(CVT).⁵⁰ Tunneling probabilities were computed using the centrifugal-dominant, small curvature, semiclassical, adiabatic, ground-state (CD-SCSAG) method.⁵⁴ The corresponding rate constants derived from these probabilities are termed TST/CD-SCSAG and CVT/CD-SCSAG for the conventional and variationally computed rate constants, respectively.

The direct dynamics calculations on 17a, 17b, and 17c each required in excess of 20 h of Cray C90 cpu time. The massive increase in computer time that would be required to study the full systems 3a–5a or 3b–5b made those computations unfeasible. The SO_2Ph groups should not affect the mechanism of double hydrogen dyotropy in syn-sesquinorbornene deriva-

(54) Liu, Y.-P.; Lynch, G. C.; Truong, T. N.; Lu, D.-H.; Truhlar, D. G.; Garrett, B. C. *J. Am. Chem. Soc.* **1993**, *115*, 2408.

Table 8. Summary of Calculated Rate Constants for **17a** Stepwise Double Hydrogen Transfer

<i>T</i> (K)	calculated rate constants ($k_2 = k_{-1}$) (s^{-1})			
	TST	CVT	TST/CD-SCSAG	CVT/CD-SCSAG
173.00	$2.3073 \times 10^{+7}$	$2.2890 \times 10^{+7}$	$1.2945 \times 10^{+10}$	$1.2953 \times 10^{+10}$
223.00	$3.2852 \times 10^{+8}$	$3.2676 \times 10^{+8}$	$2.1143 \times 10^{+10}$	$2.1167 \times 10^{+10}$
273.00	$1.7451 \times 10^{+9}$	$1.7388 \times 10^{+9}$	$3.2592 \times 10^{+10}$	$3.2641 \times 10^{+10}$
298.00	$3.2486 \times 10^{+9}$	$3.2392 \times 10^{+9}$	$3.9642 \times 10^{+10}$	$3.9707 \times 10^{+10}$
323.00	$5.4847 \times 10^{+9}$	$5.4719 \times 10^{+9}$	$4.7596 \times 10^{+10}$	$4.7676 \times 10^{+10}$
373.00	$1.2633 \times 10^{+10}$	$1.2615 \times 10^{+10}$	$6.6187 \times 10^{+10}$	$6.6299 \times 10^{+10}$
383.00	$1.4539 \times 10^{+10}$	$1.4520 \times 10^{+10}$	$7.0326 \times 10^{+10}$	$7.0444 \times 10^{+10}$
393.00	$1.6613 \times 10^{+10}$	$1.6602 \times 10^{+10}$	$7.4602 \times 10^{+10}$	$7.4768 \times 10^{+10}$
403.00	$1.8857 \times 10^{+10}$	$1.8847 \times 10^{+10}$	$7.9013 \times 10^{+10}$	$7.9179 \times 10^{+10}$
423.00	$2.3863 \times 10^{+10}$	$2.3855 \times 10^{+10}$	$8.8232 \times 10^{+10}$	$8.8393 \times 10^{+10}$
473.00	$3.9426 \times 10^{+10}$	$3.9423 \times 10^{+10}$	$1.1351 \times 10^{+11}$	$1.1361 \times 10^{+11}$
573.00	$8.3134 \times 10^{+10}$	$8.3127 \times 10^{+10}$	$1.7271 \times 10^{+11}$	$1.7253 \times 10^{+11}$

**Figure 14.** Calculated $\log k_{\text{obs}}$ versus $1/T$ for **17a–17c** for the concerted mechanism.

tives, but they do cause the reaction to become exothermic. However, the absolute value of the rate constants calculated for **17** are significantly different than those found experimentally for **3a–5a** and **3b–5b** due to the substantial differences in calculated activation energies for either concerted or stepwise double hydrogen transfer in **17a–c** as compared to **3a–5a** or **3b–5b**. The observed experimental activation energies are 27.2, 28.4, and 33.1 kcal/mol for **3a**, **4a**, and **5a**, respectively, and 24.1, 25.3, and 26.8 kcal/mol for **3b**, **4b**, and **5b**, respectively. Using the concerted mechanism, **17a** has a classical thermal calculated (PM3) activation energy of 34.5 kcal/mol; **17b** is 35.2 kcal/mol, and E_A for **17c** is 35.9 kcal/mol. The activation energies for the stepwise mechanisms are calculated (PM3) to be considerably lower than for the concerted mechanisms (**17a**, 23.4 kcal/mol; **17b**, 23.4 kcal/mol; **17c**, 24.4 kcal/mol), and with the presence of a distinct stable biradical intermediate in each case.

Inspection of Tables 6–8 and IX–XV (supplementary material) shows that the rate constants computed using TST and CVT are essentially identical. The calculated free energy maximum using CVT is shifted by an insignificant amount from that calculated by simple TST. Hence, variational effects do not affect the mechanism of double hydrogen dyotropy in *syn*-sesquiorbornenes.⁵⁰

Tunneling, on the other hand, has quite a dramatic effect on the calculated rate constants. Tables 6–8 (the same effects are seen in Tables IX–XIV of the supplementary material) show

that CD-SCSAG corrected rate constants computed using either TST or CVT show marked rate accelerations due to tunneling. The effects are largest at the lowest temperatures (-100 °C) and smallest at the highest temperatures (300 °C). For example, for the concerted mechanism at 200 °C, where the calculated rate constants are similar to those found experimentally, the calculated rate constants are

$$k_{\text{CVT}} = 3.24 \times 10^{-4} \text{ s}^{-1} \quad \text{and} \quad k_{\text{CVT/CD-SCSAG}} = 2.29 \times 10^{-3} \text{ s}^{-1}$$

which represents an increase of about 1 order of magnitude due to tunneling. Within the range of temperatures used experimentally (100–130 °C for **3–5a** and 50–100 °C for **3–5b**) it is predicted that the reaction involving **17** is dominated by tunneling.

For the experimental compounds (**3a–5a**, **3b–5b**), the magnitude of tunneling will be influenced by the presence of the SO_2Ph groups. These cause the overall reactions to become exothermic, and the vibrational levels on the reactant and product sides of the transition state to become unsymmetrical, similar to the case of the stepwise mechanism in our model reaction.

Plots of $\log(k_{\text{obs}})$ versus $1/T$ are found in Figures 14–16. For the concerted mechanism

$$k_{\text{obs}} = k_1$$

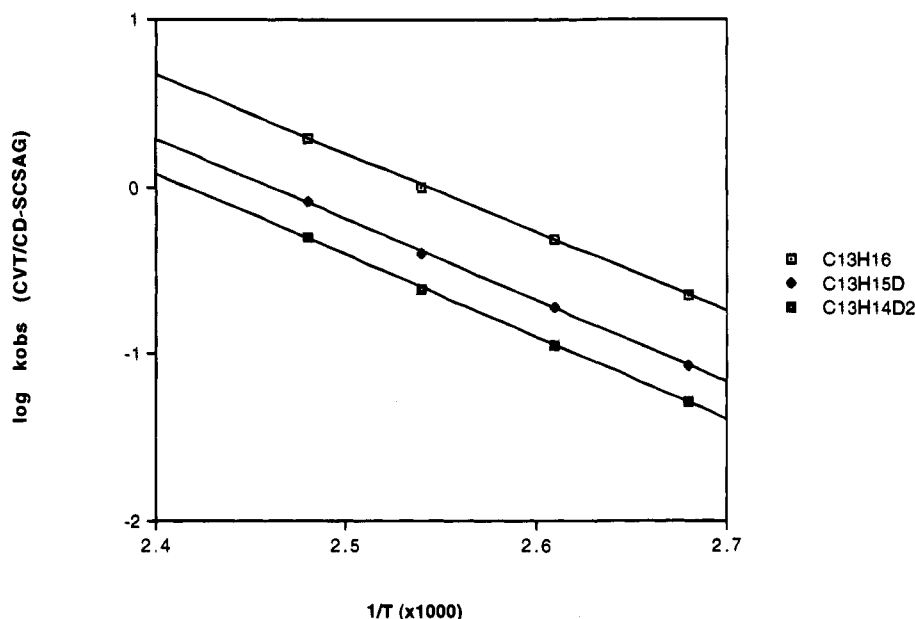


Figure 15. Calculated $\log k_{\text{obs}}$ versus $1/T$ for 17a–17c for the stepwise mechanism.

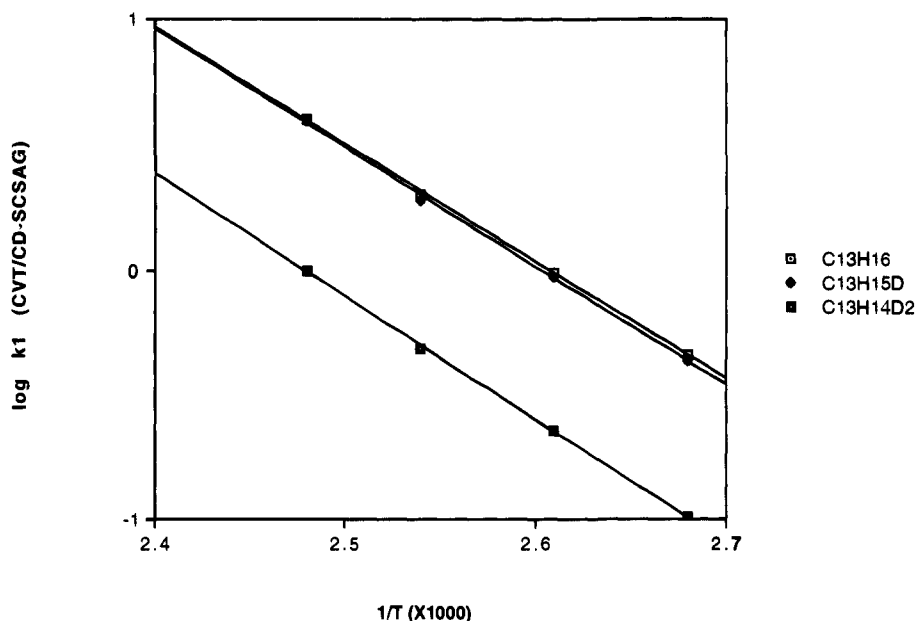


Figure 16. Calculated $\log k_{\text{obs}}$ versus $1/T$ for 17a–17c for the stepwise mechanism where $k_{\text{obs}} = k_1$.

since there is no intermediate present. For the stepwise mechanism,

$$k_{\text{obs}} = \frac{k_1 k_2}{k_{-1} + k_2}$$

where k_1 is the rate constant for the formation of 20, the transfer of the first hydrogen (deuterium); k_{-1} is the rate constant for that reverse reaction; and k_2 is the calculated rate constant for the second hydrogen (deuterium) transfer (Figure 17a).

Figure 14 shows the calculated CVT/CD-SCSAG rate constants versus $1/T$ for the concerted mechanism, within the experimental temperature range (100–130 °C). This plot is typical of what is expected for a concerted reaction.⁵⁵ The rate constants for the synchronous transfer of one hydrogen and one deuterium fall approximately midway between the calculated rate constants for either double hydrogen or double deuterium

transfer. Thus, the isotope effects are roughly multiplicative, obeying the rule of the geometric mean.²⁷ A similar relationship, that is

$$k_{\text{HH}}/k_{\text{HD}} \approx k_{\text{HD}}/k_{\text{DD}}$$

is obtained if one uses TST or CVT calculated rate constants (Tables 7 and 8) without tunneling probabilities. This implies that while tunneling is calculated to dominate the reaction, the relative isotope effects are not significantly affected by tunneling.

For the concerted mechanism, using CVT/CD-SCSAG generated rate constants at 100 °C, the $k_{\text{HH}}/k_{\text{HD}}$ isotope effect is 6.89 and the $k_{\text{HH}}/k_{\text{DD}}$ isotope effect is calculated to be 58.55. These absolute values for the isotope effects are considerably larger than those observed for 3–5 experimentally. Nevertheless, for these CVT/CD-SCSAG calculated rate constants,

$$k_{\text{HH}}/k_{\text{HD}} \approx k_{\text{HD}}/k_{\text{DD}}$$

(55) Engdahl, K.-A.; Bivehed, H.; Ahlberg, P.; Saunders, W. H., Jr. *J. Am. Chem. Soc.* **1983**, *105*, 4767.

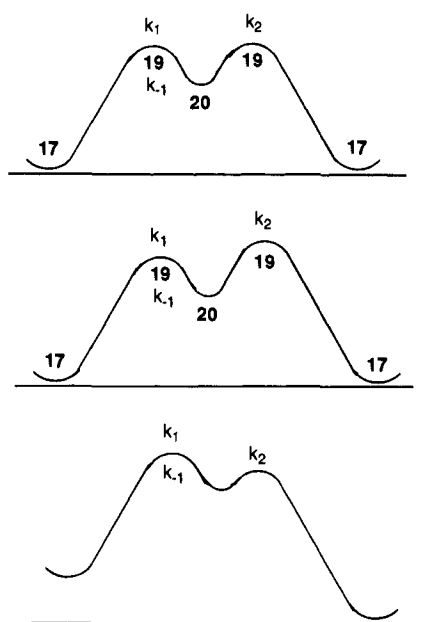


Figure 17. (a, top) Potential energy surface for model compound **17**. (b, middle) Potential energy surface for model compound **17b** corrected for differences in ZPVE. (c, bottom) Potential energy surface for an exothermic reaction.

As noted above, isotope effects calculated using CVT (or TST) rate constants without tunneling probabilities included give

$$k_{\text{HH}}/k_{\text{HD}} = 2.7 \quad \text{and} \quad k_{\text{HH}}/k_{\text{DD}} = 8.1$$

These are almost identical to those found experimentally for **3b–5b** at 100 °C where

$$k_{\text{HH}}/k_{\text{HD}} = 2.9 \quad \text{and} \quad k_{\text{HH}}/k_{\text{DD}} = 8.5$$

Not surprisingly then, the experimental log (k_{obs}) versus $1/T$ plot (Figure 2) for compounds **3b–5b** is remarkably similar in appearance to that computed for the concerted mechanism of our model compounds **17a–c** (Figure 14). In particular, the separation of the two sets of lines are nearly equivalent, that is

$$k_{\text{HH}}/k_{\text{HD}} \cong k_{\text{HD}}/k_{\text{DD}}$$

This suggests that the experimental isotope effects for **3b–5b** are consistent with a concerted mechanism. Mackenzie *et al.* also concluded that double hydrogen dytropy in their pentacyclic triene and pyrazoline systems was via a concerted mechanism.^{5a} Grimme has reached similar conclusions for his 10-electron systems.^{5d} An isotope effect study by Ahlberg and Saunders *et al.*⁵⁵ on the epimerization of tetramethylglucose (TMG) catalyzed by 2-pyridinone concluded that double hydrogen transfer in that system was also via a concerted mechanism. They also showed that the synchronous and asynchronous concerted mechanisms give rise to very similar kinetic isotope behavior, and thus they could not use kinetic isotope effects to differentiate between a synchronous and an asynchronous concerted mechanism. Furthermore, Ahlberg and Saunders were able to show that very large isotope effects (*i.e.* $k_{\text{HH}}/k_{\text{DD}} = 65.1$) were expected only in cases where there is little or no heavy-atom motion in the transition state. For a concerted mechanism where heavy atom motion was significant, they calculated, using BEBOVIB IV,⁵⁵ a $k_{\text{HH}}/k_{\text{DD}}$ isotope effect of only 3.7. Thus, they concluded that concerted double hydrogen transfers can result in a variety of observed $k_{\text{HH}}/k_{\text{DD}}$ isotope ratios depending upon the degree of heavy-atom motion along the reaction coordinate in the transition state.^{12,55}

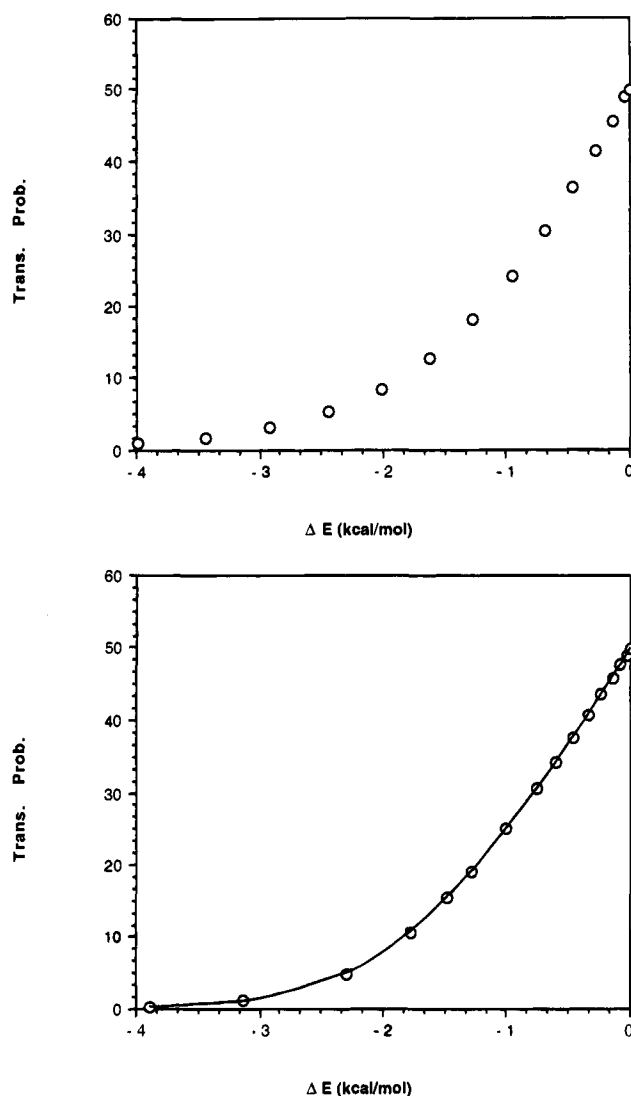


Figure 18. (a, top) Calculated tunneling transmission probabilities (%) for concerted hydrogen dytropy in **17a** as a function of change in energy relative to the transition state ($\Delta E = 0.0$ kcal/mol). (b, bottom) Calculated tunneling transmission probabilities (%) for stepwise hydrogen dytropy in **17a** as a function of change in energy relative to the transition state ($\Delta E = 0.0$ kcal/mol).

The near-perfect agreement of the CVT calculated isotope effects for **17a–c** and the experimental kinetic isotope effects for **3b–5b** suggest that tunneling is not dominant in compounds **3–5**. This is in agreement with the study by Ahlberg and Saunders which showed that tunneling was not significant for the concerted double hydrogen transfer in the epimerization of TMG by 2-pyridinone.⁵⁵ However, as the present direct dynamics calculations have shown, while individual rate constants are accelerated by the presence of quantum tunneling, the $k_{\text{HH}}/k_{\text{HD}} \cong k_{\text{HD}}/k_{\text{DD}}$ relationship is unchanged due to tunneling. The direct dynamics calculations also reveal that quantum mechanical tunneling only occurs to a significant extent at geometries very close to that of the transition state for either the concerted or stepwise mechanisms. As Figure 18 shows, tunneling probabilities are only significant near the top of the barrier for both mechanisms. This is significant and explains why the presence, or absence, of tunneling can not be used to differentiate between the concerted and stepwise mechanisms.

The experimental isotope effects for **3a–5a** (Figure 1) show a significant deviation from what would be expected for a concerted mechanism (Figure 14). Figure 15 is a plot of log (k_{obs}) CVT/CD-SCSAG calculated rate constants versus $1/T$

(within the experimental temperature range of 100–130 °C) for the stepwise mechanism depicted in the lower part of Figure 13. Interestingly, Figure 1, the experimentally observed relationship between rate constant and temperature, does not resemble the rate constant/temperature relationship as computed for the stepwise mechanism (Figure 15). In fact, Figure 15 shows that for model compound **17** the $k_{\text{HH}}/k_{\text{HD}}$ isotope effect is significantly larger than the $k_{\text{HD}}/k_{\text{DD}}$ isotope effect. This is contrary to what was found experimentally (Figure 1) where it was shown that $k_{\text{HH}}/k_{\text{HD}}$ is somewhat smaller than $k_{\text{HD}}/k_{\text{DD}}$ (for **3a–5a**).

To understand what is happening to the isotope effects in the stepwise mechanism, one must consider the relationship between the observed rate constants and the potential energy surface for a given reaction. Figure 17a shows the perfectly symmetrical MOPAC generated PES for model compound **17**. Isotopic substitution does not change this surface. However, the change in zero-point vibrational energy (ZPVE) associated with isotopic substitution will cause a perturbation of this surface, such that the new surface for **17b** will look like that depicted in Figure 17b. Clearly, when both isotopes are identical (either **17a** or **17c**) then the PES including ZPVE resembles that shown in Figure 17a, where $k_2 = k_{-1}$ so that

$$k_{\text{obs}} = k_1/2$$

However, in the case of one hydrogen and one deuterium transferring (**17b**), where the second step is the transfer of the deuterium, then

$$k_2 < k_{-1}$$

This has obvious consequences to the overall rate constant since

$$k_{\text{obs}} = \frac{k_1 k_2}{k_{-1} + k_2}$$

Thus, for any situation where k_{-1} is of comparable or greater magnitude than k_2 , the isotope effects associated with k_2 will play an important role in the overall isotope effects for the reaction.

A limiting case for this effect would be seen if $k_2 \ll k_{-1}$ (a situation only likely if the overall reaction were highly endothermic). In such a case, the isotope effect on k_2 would dominate the overall isotope effect for k_{obs} . For this example, the observed rate constants for the monodeuterium/monohydrogen reaction and the double deuterium transfer reaction would be very similar, while the observed rate constant for the double hydrogen transfer would be appreciably faster. This is similar to the situation observed for compound **17** (Figure 15). Here, the rates for monohydrogen/monodeuterium transfer (**17b**) are closer to those for the double deuterium reaction (**17c**) than for the double hydrogen reaction (**17a**). This suggests that for model compound **17b**, $k_2 < k_{-1}$, which is in fact the case as calculated by semiempirical theory (Figure 17b).

The opposite of this situation is the case where $k_2 \gg k_{-1}$. For such a case the isotope effect is manifested in the first step (k_1). This would naturally lead to very similar calculated (or observed) rate constants for **17a** and **17b**, since these both involve initial transfer of a hydrogen atom. Rate constants for **17c** would be much slower due to the decreased probability of deuterium tunneling relative to hydrogen. These results are displayed in Figure 16, where it is assumed that $k_{\text{obs}} = k_1$.

When k_2 is similar to, but somewhat greater than k_{-1} , behavior intermediate between that seen for either Figure 15 (where $k_2 < k_{-1}$) or Figure 16 (where $k_2 \gg k_{-1}$) would be predicted. This

is, in fact, exactly what is observed experimentally for compounds **3a–5a** (Figure 1). Here we see that the observed rates for the monodeuterium/monohydrogen transfer (**4a**) are closer in absolute value to those for the double hydrogen case (**3a**) than the double deuterium one (**5a**). However, this explanation is only plausible if the potential energy surface resembles that depicted in Figure 17c. This is indeed the situation for compounds **3a–5a** since the products of these reactions are lower in energy than the reactants (conjugative interaction of the SO_2Ph with the double bond) which causes the right side of the potential surface to be “pulled down” relative to the left side. In other words, the activation barrier for the second step is lower than that for the reverse of the first step (*i.e.* $k_{-1} < k_2$). Thus, the calculated rate constant ratios for the stepwise mechanism of model compound **17** suggests that double hydrogen transfer in **3a–5a** occurs via a stepwise mechanism.

It should be noted that, with the present data set, it is not possible to discern between a stepwise mechanism and a highly asynchronous concerted mechanism in which the transition state of the concerted reaction resembles the possible biradical intermediate. However, it should also be noted that we have not found any evidence for such an asynchronous concerted mechanism at either the semiempirical or *ab initio* levels of theory. Similarly, isotope effects for perfectly synchronous and slightly asynchronous concerted mechanisms are expected to be very similar, even in cases where the transferring protons are highly coupled.⁵⁵ Thus it is not possible to differentiate between a perfectly synchronous and slightly asynchronous concerted mechanism with the current data.

It should also be emphasized that although the direct dynamics calculations on model compound **17** support a concerted mechanism for the double H-dyotropy in compounds **3b–5b**, this is not unequivocal proof. In the case of a stepwise mechanism, with $k_{-1} = k_2$, the calculated dynamics for the two mechanisms (concerted and stepwise) would be indistinguishable.

For the stepwise mechanism of double hydrogen dyotropy in *syn*-sesquinorbornenes, $k_{\text{HH}}/k_{\text{HD}}$ is significantly smaller than $k_{\text{HD}}/k_{\text{DD}}$. This agrees with the observed isotope effects for **3a–5a**, implying that double hydrogen transfer in this system is via a stepwise mechanism. Conversely, the observed isotope effects for **3b–5b** agree much better with those calculated for a concerted mechanism for the model compound **17**. Although the dynamics calculations do not require this, the earlier CASSCF calculations do indicate that the concerted and stepwise reactions are nearly isoenergetic, and it is possible that a small geometrical perturbation could shift the mechanism from stepwise to concerted. In the molecules in question, this change in mechanism might occur upon changing from **3, 4, 5a** to **3, 4, 5b**. At the PM3 level of theory, compounds **3a–5a** are more extended than the corresponding compounds in the **3b–5b** series. That is, in the **3a–5a** compounds the C_2 fragments (the termini from which the hydrogens are transferred) must distort to a greater extent to achieve a synchronous concerted transition state similar to that present in the model compounds **17a–c** than do the **3b–5b** compounds. It is not unreasonable then, to postulate that the greater geometric distortion necessary to reach the concerted transition state in the **3a–5a** series results in the alternative stepwise mechanism becoming energetically favored (as depicted in Figure 9 for the ethylene–ethane system). It is important to remember that, at the best levels of theory employed herein, the two mechanisms for double H-dyotropy of **13** are extremely close in energy, and in fact after inclusion of zero-point energy effects, the two mechanism (concerted and stepwise) are calculated to have the same activation energy.

Conclusions. The dyotropic rearrangements considered here are examples of double hydrogen transfer between ethane and ethene moieties. This process has been generally assumed to take place by means of a concerted reaction mechanism, since, as pointed out by Woodward and Hoffmann, it is allowed by orbital symmetry. Recent MP2/6-31G* calculations for an imposed D_{2h} transition state⁹ predict an activation enthalpy of 48 kcal/mol, considerably lower than the earlier result of 74 kcal/mol obtained by Feller et al.⁸ who used the FORS MCSCF approach. Neither report considers the fact that hydrogen normally transfers by tunneling so that the temperature dependence of the transfer rate cannot be simply expressed in terms of an enthalpy of activation. Instead, one may calculate the rate of penetration of a one-dimensional barrier with a height equal to that calculated and a tunneling distance derived from structural information or from van der Waals radii. However, as illustrated by our calculations this often leads to barriers that are much lower than those calculated quantum-chemically.

Such calculations are ineffective in elucidating the mechanism of the transfer. Suitable parameter values can be found for concerted as well as stepwise transfer. The high activation energy allows kinetic measurements only over a narrow range of temperatures, much too narrow to observe the curvature characteristic of Arrhenius plots for tunneling reactions. Therefore, the modeling offers no reliable information on the nature of the tunneling particle, namely whether it is a single hydrogen atom as in stepwise transfer or a pair of hydrogen atoms as in concerted transfer.

To differentiate between these mechanisms, it is necessary to use a more general approach, in particular one that allows a clear separation of the motion along the reaction coordinate from the other degrees of freedom. The first model chosen to achieve this separation is a two-oscillator model based on the Golden Rule in which the transfer is formulated as a transition between (meta-) stable initial and final states. The two oscillators are the C-H oscillators of the transferring hydrogen atoms, whose properties are assumed known, and an effective skeletal vibration modulating the transfer distance, whose harmonic frequency and reduced mass are, within limits, treated as free parameters. Starting from these potentials and using the observed activation energy and exothermicity, an empirical barrier is constructed so as to fit the observed rate constants and their temperature dependence for the three isotopes of a given molecule of the present series. It is found that this model can produce good fits with reasonable parameter values which, except for the energy parameters, remain essentially the same for all molecules probed, but only if stepwise transfer is assumed. If an empirical barrier is constructed that reproduces the rate of concerted transfer for one isotope at one temperature, the rates for other isotopes and at other temperatures are found to deviate strongly from the experimental results. Specifically, it is found that the activation energy is much too low and the isotope effect is too large. If, in the limited temperature range of the experiments, the calculated concerted rate constants are written in the form of an Arrhenius equation, the frequency factor is found to be too low by many orders of magnitude. This is typical for tunneling models. If the barrier is very high in relation to kT , tunneling well below the top of the barrier is favored; hence the low activation energy and small frequency factor. In the case of stepwise transfer the lowest energy at which tunneling can occur is governed by the energy of the intermediate state; the corresponding extra expenditure of thermal energy allows tunneling of a lighter particle (one hydrogen atom rather than two) through a thinner barrier, leading to a much larger frequency factor which compensates for the higher activation

energy. In general, an increase in temperature will always shift the balance between the two mechanisms from concerted to stepwise transfer. The actual transition temperature will depend on the system at hand. The two-oscillator model indicates that this transition temperature for the molecules under consideration lies well below the temperatures of the experiment.

It is possible, however, that this result is an artifact of the model. This is suggested by the observation that the empirical barrier does not agree well with the CASSCF results. Also, the single effective mode used to represent the skeletal modes may conceivably fail to provide an adequate description of their effect on the transfer. In an attempt to obtain a more accurate picture of the dynamics, full-scale dynamics calculations were carried out on a model compound differing from **3a** by the removal of the two sulfone groups, a simplification dictated by expediency. The structure, vibrational frequencies, and the potential energy surface were calculated at the PM3 level, which is likely to produce good structures and force fields but to yield low energy barriers for the stepwise process and to overestimate the stability of the biradical intermediate.

These calculations produced results that are qualitatively similar to those of the two-oscillator model. The calculated rates for both mechanisms are dominated by tunneling transfer for both hydrogen and deuterium, occurring from highly vibrationally excited states near the top of the barrier. For stepwise transfer, the rates in the range of experimental temperatures are about 10^6 times higher than for concerted transfer. They are in fact higher than the observed rates by roughly the same factor. An Arrhenius plot of the calculated rates indicates that for stepwise transfer the activation energy is too low but the frequency factor matches the observed result. For concerted transfer, both the frequency factor and the activation energy are lower than the experimental results, indicating that the similarity of the calculated concerted rates to the observed rates is due to a compensation of errors. The dynamics results on the concerted mechanism with no tunneling corrections agree better with observed rates and isotope effects for the **3b**–**5b** series.

At a higher level of theory, the metastable biradical state disappears and exhibits a single maximum. It should be realized that the terms stepwise or highly asynchronous concerted and concerted synchronous transfer as used here represent two limits of a continuous range of transfer pathways, all of which are simultaneously operative. Stepwise transfer, such that the second hydrogen transfers only after the first has arrived and is thermally equilibrated, obviously requires a metastable intermediate with a lifetime long on the time scale of the vibrations involved. Synchronous transfer such that the two hydrogens move together in phase obviously requires two identical particles and hence cannot apply to the HD compounds. One can easily envisage a preferred pathway that is concerted in the sense that there is no identifiable intermediate but asynchronous in the sense that the two particles transfer independently, *i.e.*, out of phase.

Turning to isotope effects, one can possibly detect a move in that direction in comparing **3b**–**5b** with **3a**–**5a**. For the **a** series the mixed isotope has a rate constant k_{HD} close to k_{HH} , in agreement with the notion that tunneling of a single hydrogen atom is the rate-determining step for the preferred transfer pathway in both isotopes. This as well as the magnitude of the isotope effect is in agreement with stepwise transfer. However, this may be an oversimplification since in tunneling transitions the rate will depend on coincidences of initial and final state levels of the vibrations governing the transfer, in particular the CH/D stretching vibrations. In the case of stepwise transfer,

the coincidences are between the initial-state overtone levels and the intermediate-state zero-point level; since these will change upon deuteration, this will tend to influence the isotope effect. In the case of concerted transfer, this influence would vanish for symmetric barriers, but in the molecules studied experimentally, the barrier is always asymmetric so that the same considerations apply.

In the case of the **3b–5b** series, k_{HD} equals the geometric mean of k_{HH} and k_{DD} within experimental error. The barrier is predicted to be lower than for the **a** series, in agreement with the observed lower activation energy. The pattern and magnitudes of the deuterium isotope effects resemble those corresponding to a secondary isotope effect. The two-oscillator model does not support such an interpretation; it can be fitted satisfactorily to the observed rate constants if stepwise transfer is assumed; except for the barrier height and the experimental barrier asymmetry, the parameters differ only marginally from those from the **a** series. The direct dynamics calculations do not refer to an asymmetric barrier, but in general the asymmetry would favor tunneling since it allows transfer to more highly excited final-state levels which can penetrate the barrier more effectively. Overall, the calculations and observations suggest that the balance between concerted and stepwise transfer has shifted somewhat toward concerted transfer in the **b** series.

Considering the complexity of the molecules studied, it is not surprising that a margin of uncertainty remains in the analysis of the transfer mechanism. Nevertheless, the study shows the overriding importance of factors often overlooked in such hydrogen transfer processes, namely quantum-mechanical tunneling and asynchronous transfer which may take the form of a stepwise process via a biradical intermediate.

Experimental Section

For experimental details, see the preceding paper in this issue.

1,2-Bis(phenylthio)-1-chloroethane- d_3 (10). A solution of KOH (2.0 g, 30 mmol) in absolute ethanol (100 mL) was treated with thiophenol (3.24 g, 27 mmol) and stirred for 3 h prior to the addition of 1,2-dichloroethane- d_4 (1 mL, 12.2 mmol). This mixture was stirred at room temperature for 6 h, refluxed for 12 h, cooled, and partitioned between water (100 mL) and ether (100 mL). The separated aqueous phase was extracted with ether (3 \times 100 mL), and the combined organic phases were dried and evaporated. Purification of the residue by silica gel chromatography afforded 2.9 g (97%) of 1,2-bis(phenylthio)ethane- d_4 : $^1\text{H NMR}$ (300 MHz, CDCl_3) δ 7.40–7.05 (m, 10 H); $^{13}\text{C NMR}$ (75 MHz, CDCl_3) ppm 135.1, 130.1, 129.0, 126.6, 33.5; $^2\text{H NMR}$ (46 MHz, CH_2Cl_2) δ 3.04 (4 D); MS m/z (M^+) calcd 250.0788, obsd 250.0780.

A solution of the above product (1.00 g, 4 mmol) in CH_2Cl_2 (100 mL) was treated with *N*-chlorosuccinimide (620 mg, 4.7 mmol), stirred overnight at room temperature, and freed of solvent. This unpurified product was used directly. Purification of a small sample gave **10**: $^1\text{H NMR}$ (300 MHz, CDCl_3) δ 7.60–7.05 (m, 10 H); $^2\text{H NMR}$ (46 MHz, CH_2Cl_2) δ 4.88 (s, 1 D), 3.10 (s, 2 D).

(E)-1,2-Bis(phenylsulfonyl)ethylene-1,2- d_2 (11). A solution of unpurified **10** from above in CH_2Cl_2 (250 mL) was cooled to 0 $^\circ\text{C}$, treated slowly with 35% peracetic acid (3 mL), and stirred overnight

at room temperature. The excess peracid was quenched with aqueous sodium thiosulfate solution, and the acid was neutralized with NaHCO_3 . The product was extracted into CH_2Cl_2 (3 \times 100 mL), the combined organic layers were dried and evaporated, and the residue was recrystallized from CH_2Cl_2 –hexane to give 1.3 g (95%) of the α -chloro disulfone: mp 97–99 $^\circ\text{C}$; $^1\text{H NMR}$ (300 MHz, CDCl_3) δ 8.00–7.50 (m, 10); $^{13}\text{C NMR}$ (75 MHz, CDCl_3) ppm 135.1, 133.3, 133.2, 130.0, 129.0, 128.9, 128.1, 126.5, 57.3, 39.6; $^2\text{H NMR}$ (46 MHz, CH_2Cl_2) δ 5.2 (s, 1 D), 4.2 (s, 1 D), 3.6 (s, 1 D); MS m/z (M^+) calcd 347.0132, obsd 347.0138.

A solution of this disulfone (1.0 g, 3.0 mmol) in CH_2Cl_2 (50 mL) was treated with excess 2,4,6-collidine (2 mL), stirred at room temperature for 5 h, washed with 1% HCl and brine, dried, and evaporated. Pure **11** was obtained by silica gel chromatography (elution with CH_2Cl_2): 200 mg (80%), white solid, mp 220 $^\circ\text{C}$; $^1\text{H NMR}$ (300 MHz, CDCl_3) δ 7.99–7.50 (m, 10 H); $^{13}\text{C NMR}$ (75 MHz, CDCl_3) ppm 140.7, 138.3, 134.9, 129.9, 128.6; $^2\text{H NMR}$ (46 MHz, CH_2Cl_2) δ 7.36 (s, 2 D); MS m/z calcd 310.0302, obsd 310.0312.

(Z)-1,2-Bis(phenylsulfonyl)ethylene-1,2- d_2 (12). A deoxygenated solution of **11** (700 mg, 2.3 mmol) in CH_2Cl_2 (700 mL) containing 1-acetonaphthone (100 mg) was placed in a Pyrex test tube and irradiated in a Rayonet reactor equipped with a full bank of 3000 Å bulbs for 2 days. The solvent was evaporated, and the isomers were separated by MPLC on silica gel (elution with 1% ethyl acetate in CH_2Cl_2). There was isolated 50 mg (7%) of **12**. The mixture of **11** and 1-acetonaphthone (750 mg) was resubmitted to the conditions of irradiation. For **12**: $^1\text{H NMR}$ (300 MHz, CDCl_3) δ 7.99–7.50 (m, 10 H); $^2\text{H NMR}$ (46 MHz, CH_2Cl_2) δ 6.80 (s, 2 D); MS m/z (M^+) calcd 310.0302, obsd 310.0332.

Disulfones 4 and 5. These four substrates were prepared as previously described starting from **11** and **12**. For **4a** and **4b**, the $^2\text{H NMR}$ signal (in CH_2Cl_2 solution) was seen at δ 3.95. In the case of **5a** and **5b**, the chemical shift of the deuterium substituent(s) was only slightly more downfield (δ 3.96). The deuterium signal in the dyotropic shift isomers of **4a** and **4b** appeared at δ 1.57. For those related to **5a** and **5b**, the characteristic deuterium chemical shift was determined to be δ 1.55. All eight compounds exhibited molecular ions in their high-resolution mass spectra commensurate with the structural assignments. The remaining spectral features (IR, $^1\text{H NMR}$, $^{13}\text{C NMR}$) of these labeled compounds compared very closely to those of the parent disulfones.

Kinetic Measurements. The procedures employed for the acquisition of rate data were identical to those utilized in the preceding paper.^{6c}

Acknowledgment. The authors thank Prof. Richard Schowen and Prof. Donald Truhlar for their insightful comments, the National Institutes of Health for financial support (Grant CA-12115) to L.A.P., and the National Science Foundation for financial support to KNH. This paper is issued as NRCC No. 37287.

Supplementary Material Available: Tables IX–XV in which the calculated rate constants for **17b** and **17c** are summarized (7 pages). This material is contained in many libraries on microfiche, immediately follows this article in the microfilm version of the journal, and can be ordered from the ACS; see any current masthead page for ordering information.